Gas Separation

International Edition: DOI: 10.1002/anie.201904312
German Edition: DOI: 10.1002/ange.201904312

Robust Microporous Metal–Organic Frameworks for Highly Efficient and Simultaneous Removal of Propyne and Propadiene from Propylene

Yun-Lei Peng[+], Chaohui He[+], Tony Pham, Ting Wang, Pengfei Li, Rajamani Krishna, Katherine A. Forrest, Adam Hogan, Shanelle Suepaul, Brian Space, Ming Fang, Yao Chen, Michael J. Zaworotko, Jinping Li, Libo Li, Zhenjie Zhang,* Peng Cheng, and Banglin Chen**

Abstract: *Simultaneous removal of trace amounts of propyne and propadiene from propylene is an important but challenging industrial process. We report herein a class of microporous metal–organic frameworks (**NKMOF-1-M**) with exceptional water stability and remarkably high uptakes for both propyne and propadiene at low pressures. **NKMOF-1-M** separated a ternary propyne/propadiene/propylene (0.5 : 0.5 : 99.0) mixture with the highest reported selectivity for the production of polymer-grade propylene (99.996 %) at ambient temperature, as attributed to its strong binding affinity for propyne and propadiene over propylene. Moreover, we were able to visualize propyne and propadiene molecules in the single-crystal structure of **NKMOF-1-M** through a convenient approach under ambient conditions, which helped to precisely understand the binding sites and affinity for propyne and propadiene. These results provide important guidance on using ultramicroporous MOFs as physisorbent materials.*

Propylene (C_3H_6) is an important olefin raw material in the petrochemical industry that is widely used as an essential building block for the production of polypropylene, propylene oxide, and acrylonitrile. The worldwide production capacity of propylene had reached 120 million tons in 2017, second only to the production of ethylene.[1] The production of propylene, mainly derived from the cracking of naphtha or the fractional distillation of hydrocarbons, inevitably introduces trace amounts of propyne and propadiene as impurities, which will severely poison the catalysts used in propylene polymerization.[2] To increase the lifetime and efficiency of those expensive catalysts, the impurity (propyne + propadiene) content must be reduced to 40 ppm or less in propylene polymerization.[3] Currently, the dominant technique used to remove trace amounts of propyne and propadiene is selective hydrogenation with noble-metal catalysts, which usually suffers from some disadvantages, including the high cost and short lifetime of the catalysts, low efficiency, and possible secondary pollution.[4] Therefore, developing new approaches for the efficient and simultaneous removal of trace amounts of propyne and propadiene is of great significance and urgently needed.

Separation strategies based on physical adsorption are attracting widespread attention owing to their environmentally friendly nature and energy efficiency. However, the use of traditional porous materials, such as zeolites,[5,6] and activated carbon[7] to separate ternary propyne/propadiene/propylene gas mixtures has not been realized yet, possibly because of the similar physical properties, structure, and molecular sizes of propyne, propadiene, and propylene (Scheme 1).[8] In the past two decades, metal–organic frameworks (MOFs) have emerged as a new class of porous materials and demonstrated great potential to overcome the limits of conventional porous materials (e.g. monotonous

[*] Y.-L. Peng,[+] T. Wang, Prof. Z. Zhang, Prof. P. Cheng
College of Chemistry, Nankai University
Tianjin, 300071 (P. R. China)
E-mail: zhangzhenjie@nankai.edu.cn
Prof. L. Li, Prof. B. Chen
Department of Chemistry, University of Texas at San Antonio
One UTSA Circle, San Antonio, TX 78249-0698 (USA)
E-mail: banglin.chen@utsa.edu
C. He,[+] Prof. J. Li, Prof. L. Li
College of Chemistry and Chemical Engineering
Taiyuan University of Technology
Taiyuan, 030024, Shanxi (P. R. China)
E-mail: lilibo908@hotmail.com
Prof. Z. Zhang, Prof. P. Cheng
Key Laboratory of Advanced Energy Materials Chemistry (MOE)
Nankai University, Tianjin 300071 (P. R. China)
P. Li, M. Fang
Department of Chemistry
Hebei Normal University of Science and Technology
Qinhuangdao, 066004, Hebei (China)
Prof. Y. Chen, Prof. Z. Zhang
State Key Laboratory of Medicinal Chemical Biology
Nankai University, Tianjin 300071 (P. R. China)
T. Pham, K. A. Forrest, A. Hogan, S. Suepaul, Prof. B. Space
Department of Chemistry, University of South Florida
4202 East Fowler Avenue, CHE205, Tampa, FL 33620-5250 (USA)
Prof. M. J. Zaworotko
Department of Chemical Sciences, Bernal Institute
University of Limerick
Limerick V94T9PX (Republic of Ireland)
Prof. R. Krishna
Van't Hoff Institute for Molecular Sciences, University of Amsterdam
Science Park 904, 1098 XH Amsterdam (The Netherlands)
[+] These authors contributed equally to this work.
Supporting information and the ORCID identification number(s) for the author(s) of this article can be found under: https://doi.org/10.1002/anie.201904312.

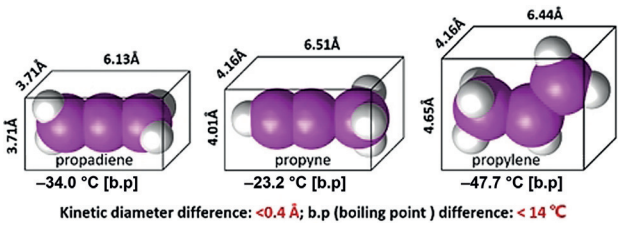

Scheme 1. Molecular structure and physical properties of propyne, propadiene, and propylene (b.p. = boiling point).

structure, lack of specific binding sites) owing to their well-defined structure, fine-tunable pore size, and custom-designed functional groups.[9–13] Much effort has been devoted to the use of MOFs for the separation of binary gas mixtures, such as acetylene/ethylene,[14–19] ethylene/ethane,[14,20–22] carbon dioxide/methane,[23,24] carbon dioxide/nitrogen,[25,26] acetylene/carbon dioxide,[27,28] krypton/xenon,[29] propyne/propylene,[30,31] and propylene/propane.[32] However, the simultaneous removal of propyne and propadiene from propylene using MOFs as absorbents is still underexplored.[8] Exploring new MOF adsorbents to simultaneously remove propyne and propadiene from propylene is of great importance for the industrial production of highly pure propylene.

$Cu[M(pdt)_2]$ (pdt = pyrazine-2,3-dithiol, M = Cu, Ni) materials were prepared by previously reported procedures.[19] **NKMOF-1-M** exhibits a three-dimensional (3D) framework constructed by four-connected $[M(pdt)_2]^-$ building blocks (Figure 1). **NKMOF-1-M** possesses one-dimensional (1D) square channels with a pore size around 5.7 Å (after subtracting van der Waals radii) along the *c* direction. Interestingly, conjugated pyrazines and metal centers (Cu or Ni) located on the wall of the 1D channels can provide two distinct binding sites for gas molecules (Figure 1), which could be beneficial for gas capture or separation applications.[19]

Notably, **NKMOF-1-M** (M = Ni or Cu) can still retain its porosity and crystallinity after soaking in water for more than 1 year at room temperature, as verified by powder X-ray diffractometry (PXRD) and BET surface-area measurements (see Figures S1–S3 in the Supporting Information). N_2 sorption isotherms collected at 77 K revealed that **NKMOF-1-Ni** and **-Cu** possessed similar BET surface areas (374 and 382 $m^2 g^{-1}$, respectively) and almost identical pore sizes (ca. 5.4 Å; Figure 2a). To explore the potential of **NKMOF-1-Ni** and **-Cu** for simultaneous ternary (propyne, propadiene, and propylene) gas mixture separation, we collected single-component gas-adsorption data of propyne, propadiene, and propylene at different temperatures (273, 298, 308, and 318 K; Figure 2b; see also Figure S4). We found that **NKMOF-1-Ni** and **-Cu** can adsorb 3.5 and 3.3 mmol g^{-1} of propyne and 3.3

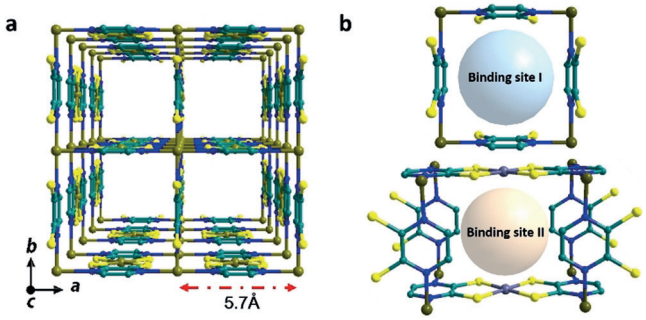

Figure 1. a) The 3D structure of **NKMOF-1-M** with 1D channels along the *c* axis. b) The two distinct binding sites in **MKMOF-1-M**. Atom colors: C teal, N blue, S yellow, Cu turquoise, Ni blue gray.

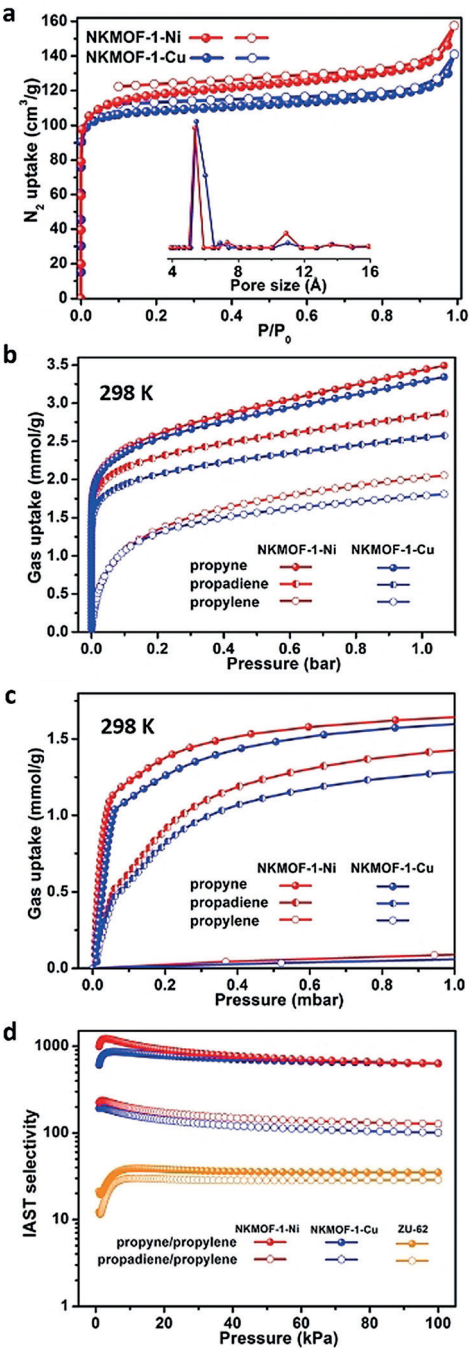

Figure 2. a) N_2 adsorption isotherms at 77 K and pore size distributions of **NKMOF-1-M**. b) Propyne, propadiene, and propylene adsorption isotherms at 1 bar and 298 K. c) Propyne, propadiene, and propylene adsorption isotherms at 1 mbar and 298 K. d) IAST selectivities of the ternary mixture (propyne/propadiene/propylene 0.5 / 0.5 / 99, v/v/v) for **NKMOF-1-M** as compared with current benchmark material (**ZU-62**) at 298 K.

and 3.0 mmol g^{-1} of propadiene at 1.0 bar and 298 K, which is much higher than the uptake of propylene (2.1 and 1.8 mmol g^{-1}, respectively). Notably, the propyne and propadiene adsorption of the two adsorbents exhibited steep curves in the low-pressure region at all tested temperatures (273, 298, 308, and 318 K), indicative of their strong binding affinity for propyne and propadiene. Gas adsorption selectivity is usually closely related to the adsorption behavior in the low-pressure region. Thus, we closely examined the adsorption behavior for each gas in the low-pressure region at 298 K (Figure 2c; see also Figure S5). Notably, **NKMOF-1-M** showed remarkably high uptake for both propadiene and propyne in the ultra-low-pressure region. For example, at pressures up to 1 mbar, the propadiene-uptake capacity of **NKMOF-1-Ni** and **-Cu** reached record values (1.43 and 1.30 mmol g^{-1}, respectively, at 1 mbar) that surpassed those of current benchmark adsorbents (see Figure S5b).[8] Furthermore, at pressures below 0.1 mbar, **NKMOF-1-M** also possessed the highest propyne capacity (1.21 and 1.10 mmol g^{-1} for **NKMOF-1-Ni** and **-Cu**, respectively, at 0.1 mbar). Meanwhile, the uptake capacity of propylene was relatively low (< 0.08 mmol g^{-1}) for **NKMOF-1-Ni** and **-Cu** below 1 mbar. This remarkable propyne and propadiene adsorption behavior in the ultra-low-pressure region indicated remarkably strong gas–sorbent interactions and high selectivity over propylene for **NKMOF-1-M**.

The isosteric enthalpy of adsorption (Q_{st}) can quantitatively represent the binding affinity of sorbents towards gases. Thus, the adsorption isotherms of single-component gases were fitted with the dual-site Langmuir–Freundlich (DSLF) isotherm model (see Tables S1–S6 in the Supporting Information). The Q_{st} value of propyne was then calculated by the DSLF method[34,35] (see Tables S7–S11), which afforded the results of 65.1 and 67.2 kJ mol^{-1} for **NKMOF-1-Ni** and **-Cu**, respectively, at zero coverage (see Figure S6). Although the obtained Q_{st} curve shapes are uncommon owing to difficulties in extracting reasonable Q_{st} values from empirical fitting (see the Supporting Information for an explanation), the zero-coverage Q_{st} values for both MOFs are close to the corresponding adsorption energies that were calculated for propyne for the primary binding site through density functional theory (DFT), as explained later. The same calculation methods afforded Q_{st} values of propadiene (54.0 and 45.2 kJ mol^{-1}) and propylene (38.0 and 37.2 kJ mol^{-1}) for **NKMOF-1-Ni** and **-Cu** (see Figures S7 and S8). These results manifest that **NKMOF-1-M** possesses much stronger binding affinity for propyne and propadiene than propylene. Overall, owing to the remarkably high uptakes and strong binding affinity for propyne and propadiene, **NKMOF-1-M** possessed great potential to simultaneously remove trace propyne and propadiene from propylene.

To evaluate the separation performance of the adsorbent materials, we calculated ternary-gas-mixture (propadiene/propyne/propylene 0.5 : 0.5 : 99, v/v/v) selectivity using ideal adsorption solution theory (IAST). The propadiene/propylene and propyne/propylene selectivity of **NKMOF-1-Ni** ranged from 127.5 to 236.5, and 630.4 to 1217.8, respectively, at 1–100 kPa (Figure 2d; see also Table S12). The selectivities of **NKMOF-1-Cu** were slightly lower than those of **NKMOF-1-Ni**, ranging from 100.8 to 193.4 for propadiene/propylene and 610.5 to 859.5 for propyne/propylene. Notably, the selectivity of both **NKMOF-1-Ni** and **NKMOF-1-Cu** are more than a magnitude higher than that of the benchmark material **ZU-62** (11.5–30.0 for propadiene/propylene and 21.3–38.9 for propyne/propylene at 1–100 kPa; Figure 2d). Thus, **NKMOF-1-Ni** and **-Cu** offer new benchmark selectivities with respect to propadiene/propyne/propylene separation.

To gain deep insight into binding sites of propyne and propadiene in the **NKMOF-1-M** platform, we obtained the crystal structure of **NKMOF-1-Cu** capturing propyne (**propyne@NKMOF-1-Cu**) and propadiene (**propadiene@NKMOF-1-Cu**), in which we could precisely study the binding sites of gas molecules with the framework of **NKMOF-1-M** and verify the results of the simulation study. Activated **NKMOF-1-Cu** crystals suitable for single-crystal X-ray diffraction (SCXRD) were placed in the corresponding gas atmosphere at room temperature with propyne or propadiene balloons, respectively. SCXRD data were then collected at 120 K, as controlled by purging with liquid nitrogen. Interestingly, structural solution showed that propyne and propadiene molecules with full site occupancy were located between the four pyrazine rings (Figure 3). This result is consistent with the strong binding site I (Figure 1b; see also Figures S9a and S9c) determined by the modeling study. Additionally, we found the propyne molecule formed strong hydrogen bonds ($HC{\equiv}C\text{-}CH_3\cdots S$, $HC{\equiv}C\text{-}CH_3\cdots C$) with the two sulfur atoms and one carbon atom of the pyrazine ring (H···S, H···C distances are 3.02, 2.95, and 2.88 Å, respectively). The propadiene molecule also formed strong hydrogen bonds ($H_2C{=}C{=}CH_2\cdots S$, $H_2C{=}C{=}CH_2\cdots C$) with the two sulfur atoms and one carbon atom of the pyrazine ring (H···S distances are 3.17, 3.13, and 3.19 Å, respectively). Propyne and propadiene molecules do not appear at the weaker binding site II. This

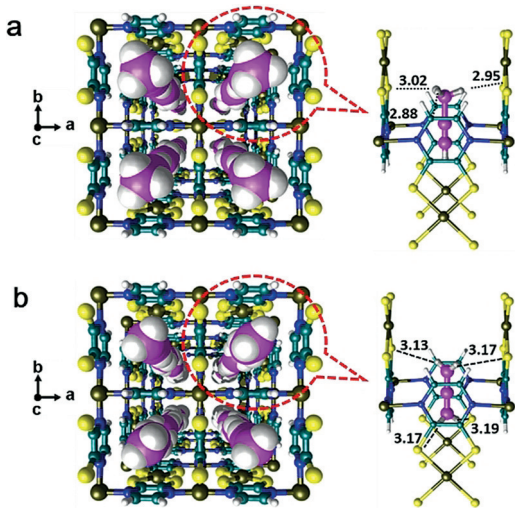

Figure 3. a) Single-crystal structure of **propyne@NKMOF-1-Cu** with propyne molecules orderly located in the 1D channels. b) Single-crystal structure of **propadiene@NKMOF-1-Cu** with propadiene molecules orderly located in the 1D channels. Atom colors: C(MOF) teal, C(propyne and propadiene) pink, H white, N blue, S yellow, Cu gold.

result confirms that propyne and propadiene preferentially bind to site I under ambient condition.

Periodic DFT calculations were performed to evaluate the propyne, propadiene, and propylene adsorption sites and energies in **NKMOF-1-M**. The DFT calculations revealed that both adsorbate molecules, propyne and propadiene, prefer to localize at two sites: 1) between four neighboring pyrazine units, and 2) between the open metal sites of two adjacent MS_4 units (see Figures S9 and S10). The region between the pyrazine units is a highly favorable binding site for the propyne and propadiene molecules in both MOFs. As the propyne and propadiene molecules are adsorbed at this site, π–π interactions between the adsorbate molecule and the surrounding pyrazine units are expected, along with H···S hydrogen-bonding interactions with the nearby S atoms. For propyne in **NKMOF-1-Cu**, the three H···S ($HC{\equiv}C\text{-}CH_3\cdots S$) bonding distances are 2.77, 2.77, and 2.85 Å (see Figure S9a). For propadiene, the four H···S ($H_2C{=}C{=}CH_2\cdots S$) bonding distances are 3.02, 2.96, 2.92, and 2.87 Å in **NKMOF-1-Cu** (see Figure S9c). Such H···S distances for both adsorbates are in reasonable agreement with those observed in the MOF through single–crystal X-ray diffraction (Figure 3). The corresponding distances in **NKMOF-1-Ni** are somewhat shorter than those obtained for **NKMOF-1-Cu**, which indicates that **NKMOF-1-Ni** exhibits greater interactions with the propyne and propadiene molecules at this site.

Comparison of the H···S bonding distances for propyne and propadiene at site I for both MOFs revealed that such distances for propyne are all shorter than those of propadiene, which indicates that propyne molecules have stronger host–guest interactions with **NKMOF-1-M** and is consistent with the results of the single-component adsorption isotherms (Figure 2c). The calculated adsorption energies for propyne at site I in **NKMOF-1-Ni** and **NKMOF-1-Cu** are −72.3 and −71.3 kJ mol^{-1}, respectively, whereas those for propadiene at the same site are −68.1 and −64.5 kJ mol^{-1}, respectively (see Tables S13 and S14). At site II in both MOFs, a favorable interaction exists between the negatively charged C atoms of the alkyne moiety and the positively charged metal ions of the MS_4 units (see Figures S9 and S10). Hydrogen-bonding interactions also occur between the H atoms of the adsorbate and the nearby S atoms of the framework at this site. Adsorption energies of −47.2 and −51.1 kJ mol^{-1} were calculated for propyne at site II in **NKMOF-1-Ni** and **-Cu**, respectively, whereas adsorption energies of −43.7 and −48.2 kJ mol^{-1} were calculated for propadiene at the same site in the respective MOFs (see Tables S13 and S14). GCMC simulations indicate that saturation of propyne and propadiene in **NKMOF-1-M** occurred at 2.5 molecules per unit cell (see Figures S11–S14). The experimental saturated adsorption data for propyne and propadiene of **NKMOF-1-Ni** (ca. 2.3 molecules per unit cell for propyne and 2.2 molecules per unit cell for propadiene at 1 bar; see Figures S14 and S15) agreed well with the simulated result. The adsorption of propylene at site I in the two MOFs is less energetically favorable than that of propyne and propadiene at this site, with calculated adsorption energies of −59.0 and −57.0 kJ mol^{-1} for **NKMOF-1-Ni** and **-Cu**, respectively (see Tables S13 and S14).

Transient breakthrough simulations were performed to evaluate the polymer-grade propylene (propyne + propadiene < 40 ppm) productivities of the tested MOFs for the separation of a ternary 0.5 : 0.5 : 99 propyne/propadiene/propylene mixture under industrial conditions. The outlet concentrations of propyne + propadiene exiting the fixed bed with these MOFs materials were evaluated as a function of the dimensionless time, τ, at 1 bar and 298 K (see Figure S20). When the outlet concentration of propyne + propadiene was less 40 ppm, the results were consistent with IAST selectivity, and the τ break value for **NKMOF-1-Ni** and **-Cu** was much longer than for other benchmark materials (hierarchy of the τ break value: **NKMOF-1-Ni** > **NKMOF-1-Cu** > **ZU-62**). Moreover, **NKMOF-1-Ni** and **NKMOF-1-Cu** possess the highest and second-highest propylene productivities of up to 191.1 and 163.3 mol L^{-1} (see Figure S20b and Table S12). The separation performance of adsorbents in the industrial fixed-bed adsorber was evaluated not only in terms of gas-mixture selectivity, but also productivity for the desired gases. Thus, **NKMOF-1-M** demonstrated excellent propyne/propadiene/propylene separation performance surpassing that of current benchmark materials, and was established as a unique MOF platform for both high selectivity and propylene productivity.

To evaluate the feasibility of ternary mixture (propyne/propadiene/propylene) separation on the tested MOFs under kinetic conditions, we performed breakthrough experiments, which are strongly pertinent to the vacuum swing adsorption (VSA) process, an energetically efficient method for industrial-scale separation. In the breakthrough experiments on an in-house-constructed separation apparatus[1] (see Scheme S1 in the Supporting Information), propyne/propadiene/propylene (0.5 : 0.5 : 99) mixtures were used as feeds to mimic the industrial process conditions. As we expected from the single-component adsorption isotherms, **NKMOF-1-Ni** displayed the best propyne/propadiene/propylene separation ability at 298 K. Propylene was first eluted through the bed, while propyne and propadiene were still adsorbed, thus affording pure polymer-grade propylene with nondetectable propyne and propadiene, and **NKMOF-1-Ni** retained propylene for a remarkable time before the breakthrough of propadiene and propyne (Figure 4a). After a certain period of time, propadiene and propyne were eluted from the column and quickly reached equilibrium. The retention time of pure propylene (propyne + propadiene < 40 ppm) for the propyne/propadiene/propylene (0.5 : 0.5 : 99) mixture on **NKMOF-1-Ni** reached 1825 min g^{-1}, which is more than 1.5 times higher than that of the benchmark MOF material, **ZU-62** (701 min g^{-1}). Notably, the performance of **NKMOF-1-Ni** is also much better than that of commercial zeolite 5A (3 min g^{-1}) and Zeolite 4A (0 min g^{-1}). The hierarchy of retention time is **NKMOF-1-Ni** > **NKMOF-1-Cu** > **ZU-62** > **zeolite 5A** > **zeolite 4A** under the same conditions (Figure 4; see also Figure S21). Moreover, such excellent propyne/propadiene/propylene (0.5 : 0.5 : 99) breakthrough performance on **NKMOF-1-M** was closely associated with its ultrahigh propyne/propylene and propadiene/propylene IAST selectivity at room temperature. The productivity of pure propylene (propyne + propadiene < 40 ppm) captured from the mixture in **NKMOF-1-Ni** and **-Cu** was as high as 230

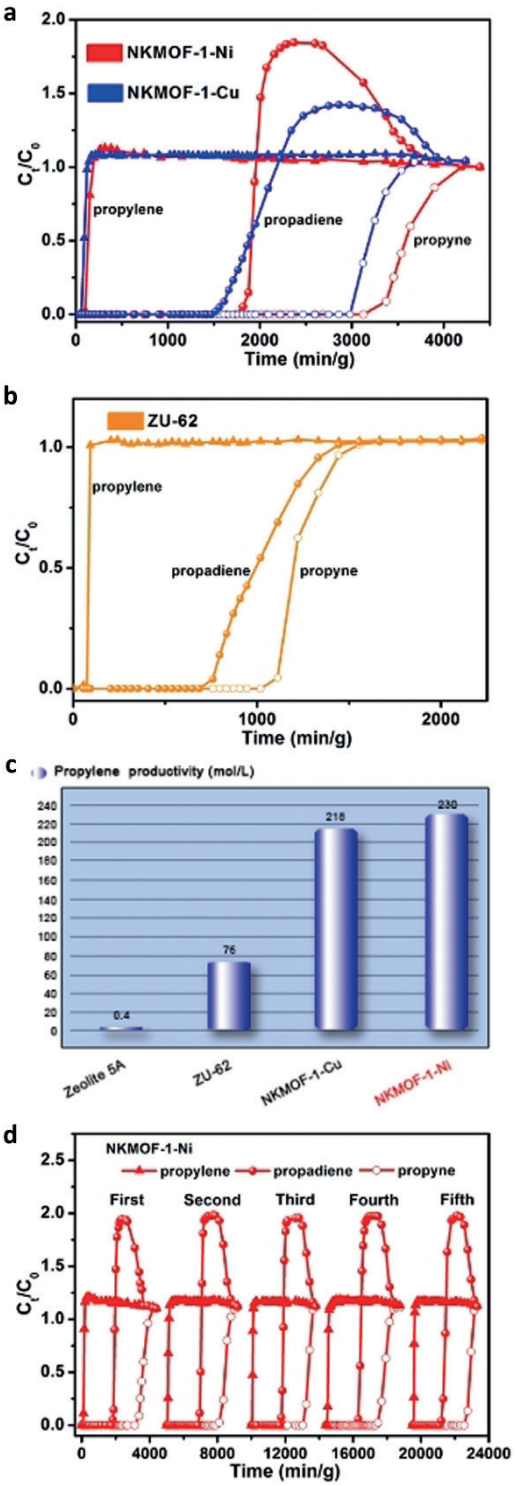

Figure 4. a) Breakthrough curves of **NKMOF-1-Ni** (red) and **NKMOF-1-Cu** (blue) for propyne/propadiene/propylene (0.5 : 0.5 : 99) mixtures. b) Breakthrough curves of the previous benchmark material, **ZU-62** (orange). c) Propylene productivity of benchmark materials. d) Breakthrough cycling test of **NKMOF-1-Ni**. Propylene: triangles, propadiene: solid circles, propyne: empty circles.

and 216 mol L^{-1}, which created new benchmarks (Figure 4c; see also Table S15).

To investigate the reusability and structural stability of **NKMOF-1-M** (M = Ni or Cu), cycling breakthrough experiments for propyne/propadiene/propylene (0.5 : 0.5 : 99) mixtures were carried out with **NKMOF-1-Ni** under the same conditions as described above in association with PXRD measurement. Owing to the inconvenient activation conditions, experiments were not carried out with **NKMOF-1-Cu**. The breakthrough curves for the ternary mixture (propyne/propadiene/propylene 0.5 : 0.5 : 99) over five cycles almost overlapped (Figure 4d), and the crystallinity of **NKMOF-1-Ni** was retained (see Figure S1), which is indicative of the excellent regenerability and stability of **NKMOF-1-Ni**.

In summary, we developed a class of robust microporous MOFs (**NKMOF-1-M**, M = Cu or Ni) with strong binding affinity for both propyne and propadiene. **NKMOF-1-M** displayed remarkably high uptake for both propyne and propadiene: the highest yet observed at ultralow pressure and room temperature. These results made **NKMOF-1-M** the best MOF adsorbents to separate propyne and propadiene from propylene. The selectivities of **NKMOF-1-Ni** and **-Cu** are more than a magnitude higher than that of the benchmark material, **ZU-62**. Both the simulated and experimental ternary-gas-mixture breakthrough results confirmed the excellent propyne/propadiene/propylene separation performance of **NKMOF-1-M**. This study provides important guidance on designing adsorbent materials with strong binding affinity for propyne and propadiene through tailoring pore aperture and introducing strong gas-sorbent interactions, such as hydrogen-bonding interactions and π–π interactions. It also paves a new avenue for the design of adsorbent materials for the simultaneous removal of multicomponent gas mixtures.

Acknowledgements

This research was supported financially by the National Natural Science Foundation of China (21601093), the National Science Foundation (Award No. DMR-1607989), including support from the Major Research Instrumentation Program (Award No. CHE-1531590), and through an ACS Petroleum Research Fund grant (ACS PRF 56673-ND6). Computational resources were made available by a XSEDE Grant (No. TG-DMR090028) and by Research Computing at the University of South Florida.

Conflict of interest

The authors declare no conflict of interest.

Keywords: binding sites · gas separation · metal–organic frameworks · physisorption · propylene purification

How to cite: *Angew. Chem. Int. Ed.* **2019**, *58*, 10209–10214
Angew. Chem. **2019**, *131*, 10315–10320

[1] L. Li, R.-B. Lin, R. Krishna, X. Wang, B. Li, H. Wu, J. Li, W. Zhou, B. Chen, *J. Am. Chem. Soc.* **2017**, *139*, 7733–7736.

[2] K. Buckl, A. Meiswinkel, *Ullmann's Encyclopedia of Industrial Chemistry*, Wiley-VCH, Weinheim, **2002**, pp. 337 – 340.
[3] A. J. McCue, A. Guerrero-Ruiz, I. Rodríguez-Ramos, J. A. Anderson, *J. Catal.* **2016**, *340*, 10 – 16.
[4] D. Teschner, J. Borsodi, A. Wootsch, Z. Révay, M. Hävecker, A. Knop-Gericke, S. D. Jackson, R. Schlögl, *Science* **2008**, *320*, 86 – 89.
[5] K. Kusakabe, T. Kuroda, A. Murata, S. Morooka, *Chem. Res.* **1997**, *36*, 649 – 655.
[6] Y. Yan, M. E. Davis, G. R. Gavalas, *Ind. Eng. Chem. Res.* **1995**, *34*, 1652 – 1661.
[7] H. Yang, Z. Xu, M. Fan, R. Gupta, R. B. Slimane, A. E. Bland, I. Wright, *J. Environ. Sci.* **2008**, *20*, 14 – 27.
[8] L. Yang, X. Cui, Z. Zhang, Q. Yang, Z. Bao, Q. Ren, H. Xing, *Angew. Chem. Int. Ed.* **2018**, *57*, 13145 – 13149; *Angew. Chem.* **2018**, *130*, 13329 – 13333.
[9] K. Adil, Y. Belmabkhout, R. S. Pillai, A. Cadiau, P. M. Bhatt, A. H. Assen, G. Maurin, M. Eddaoudi, *Chem. Soc. Rev.* **2017**, *46*, 3402 – 3430.
[10] R.-B. Li, S. Xiang, H. Xing, W. Zhou, B. Chen, *Coord. Chem. Rev.* **2019**, *378*, 87 – 103.
[11] X. Zhao, Y. Wang, D.-S. Li, X. Bu, P. Feng, *Adv. Mater.* **2018**, *30*, 1705189.
[12] P. Li, N. A. Vermeulen, C. D. Malliakas, D. A. Gómez-Gualdrón, A. J. Howarth, B. L. Mehdi, A. Dohnalkova, N. D. Browning, M. O'Keeffe, O. K. Farha, *Science* **2017**, *356*, 624 – 627.
[13] O. Delgado-Friedrichs, S. T. Hyde, M. O'Keeffe, O. M. Yaghi, *Struct. Chem.* **2017**, *28*, 39 – 44.
[14] E. D. Bloch, W. L. Queen, R. Krishna, J. M. Zadrozny, C. M. Brown, J. R. Long, *Science* **2012**, *335*, 1606 – 1610.
[15] M. L. Aubrey, M. T. Kapelewski, J. F. Melville, J. Oktawiec, D. Presti, L. Gagliardi, J. R. Long, *J. Am. Chem. Soc.* **2019**, *141*, 5005 – 5013.
[16] X. Cui, K. Chen, H. Xing, Q. Yang, R. Krishna, Z. Bao, H. Wu, W. Zhou, X. Dong, Y. Han, B. Li, Q. Ren, M. J. Zaworotko, B. Chen, *Science* **2016**, *353*, 141 – 144.
[17] R. Matsuda, R. Kitaura, S. Kitagawa, Y. Kubota, R. V. Belosludov, T. C. Kobayashi, H. Sakamoto, T. Chiba, M. Takata, Y. Kawazoe, Y. Mita, *Nature* **2005**, *436*, 238 – 241.
[18] S. Yang, A. J. Ramirez-Cuesta, R. Newby, V. Garcia-Sakai, P. Manuel, S. K. Callear, S. I. Campbell, C. C. Tang, M. Schröder, *Nat. Chem.* **2014**, *7*, 121 – 129.
[19] Y.-L. Peng, T. Pham, P. Li, T. Wang, Y. Chen, K.-J. Chen, K. A. Forrest, B. Space, P. Cheng, M. J. Zaworotko, Z. Zhang, *Angew. Chem. Int. Ed.* **2018**, *57*, 10971 – 10975; *Angew. Chem.* **2018**, *130*, 11137 – 11141.
[20] P.-Q. Liao, W.-X. Zhang, J.-P. Zhang, X.-M. Chen, *Nat. Commun.* **2015**, *6*, 8697.
[21] O. T. Qazvini, R. Babarao, Z.-L. Shi, Y.-B. Zhang, S. G. Telfer, *J. Am. Chem. Soc.* **2019**, *141*, 5014 – 5020.
[22] R.-B. Lin, L. Li, H.-L. Zhou, H. Wu, C. He, S. Li, R. Krishna, J. Li, W. Zhou, B. Chen, *Nat. Mater.* **2018**, *17*, 1128 – 1133.
[23] K.-J. Chen, D. G. Madden, T. Pham, K. A. Forrest, A. Kumar, Q.-Y. Yang, W. Xue, B. Space, J. J. Perry IV, J.-P. Zhang, X.-M. Chen, M. J. Zaworotko, *Angew. Chem. Int. Ed.* **2016**, *55*, 10268 – 10272; *Angew. Chem.* **2016**, *128*, 10424 – 10428.
[24] J.-B. Lin, W. Xue, J.-P. Zhang, X.-M. Chen, *Chem. Commun.* **2011**, *47*, 926 – 928.
[25] O. Shekhah, Y. Belmabkhout, Z. Chen, V. Guillerm, A. Cairns, K. Adil, M. Eddaoudi, *Nat. Commun.* **2014**, *5*, 4228.
[26] Y.-S. Bae, O. K. Farha, J. T. Hupp, R. Q. Snurr, *J. Mater. Chem.* **2009**, *19*, 2131 – 2134.
[27] R.-B. Lin, L. Li, H. Wu, H. Arman, B. Li, R.-G. Lin, W. Zhou, B. Chen, *J. Am. Chem. Soc.* **2017**, *139*, 8022 – 8028.
[28] B. Li, B. Chen, *Chem* **2016**, *1*, 669 – 671.
[29] D. Banerjee, C. M. Simon, S. K. Elsaidi, M. Haranczyk, P. K. Thallapally, *Chem* **2018**, *4*, 466 – 494.
[30] L. Yang, X. Cui, Q. Yang, S. Qian, H. Wu, Z. Bao, Z. Zhang, Q. Ren, W. Zhou, B. Chen, H. Xing, *Adv. Mater.* **2018**, *30*, 1705374.
[31] L. Li, H.-M. Wen, C. He, R.-B. Lin, R. Krishna, H. Wu, W. Zhou, J. Li, B. Li, B. Chen, *Angew. Chem. Int. Ed.* **2018**, *57*, 15183 – 15188; *Angew. Chem.* **2018**, *130*, 15403 – 15408.
[32] A. Cadiau, K. Adil, P. M. Bhatt, Y. Belmabkhout, M. Eddaoudi, *Science* **2016**, *353*, 137 – 140.
[33] A. L. Myers, J. Prausnitz, *AIChE J.* **1965**, *11*, 121 – 127.
[34] T. Pham, K. A. Forrest, D. M. Franz, Z. Guo, B. Chen, B. Space, *Phys. Chem. Chem. Phys.* **2017**, *19*, 18587 – 18602.
[35] B. Li, Y. Zhang, R. Krishna, K. Yao, Y. Han, Z. Wu, D. Ma, Z. Shi, T. Pham, B. Space, J. Liu, P. K. Thallapally, J. Liu, M. Chrzanowski, S. Ma, *J. Am. Chem. Soc.* **2014**, *136*, 8654 – 8660.

Manuscript received: April 8, 2019
Accepted manuscript online: May 6, 2019
Version of record online: June 24, 2019

Angewandte Chemie
Eine Zeitschrift der Gesellschaft Deutscher Chemiker

Supporting Information

Robust Microporous Metal–Organic Frameworks for Highly Efficient and Simultaneous Removal of Propyne and Propadiene from Propylene

Yun-Lei Peng[+], Chaohui He[+], Tony Pham, Ting Wang, Pengfei Li, Rajamani Krishna, Katherine A. Forrest, Adam Hogan, Shanelle Suepaul, Brian Space, Ming Fang, Yao Chen, Michael J. Zaworotko, Jinping Li, Libo Li, Zhenjie Zhang,* Peng Cheng, and Banglin Chen**

anie_201904312_sm_miscellaneous_information.pdf

Materials and Methods

General Methods

Pyrazine (99%, innochem), $Cu(NO_3)_2 \cdot 3H_2O$ (Analytical reagent, Gerhardite), $(NH4)_2 \cdot SiF6$ (Analytical reagent, Greagent), 4,4'-bipyridylacetylene (95+%, HUAWEIRUIKE), $Ni(BF_4)_2 \cdot 6H_2O$ (Energy chemical), 2,3-dichloropyrazine (98%, Bide Pharmatech Ltd), Sodium hydroxide (NaOH, 97%, Aladdin), Sodium hydrosulfide (NaHS, LiDeShi), Copper(II) perchlorate hexahydrate ($Cu(ClO_4)_2.6H_2O$, 98%, Strem Chemical, Inc.), Nickel(II) perchlorate hexahydrate ($Ni(ClO_4)_26H_2O$, reagent-grade, alfa), Copper(I) iodide (CuI, >99.5%, aladdin), iodide (I_2, AR, TIANJINGFENGCHUAN), acetonitrile, ether and acetone were purchased and used without further purification. He, N_2, C_3H_4, C_3H_6, and C_2H_2 were purchased from AIR LIQUIDE. The powder X-ray diffraction data were obtained on ULTIMA IV. Fourier transform infrared spectra (FT-IR) were recorded on Nicolet IS10.

Powder X-ray diffraction (PXRD) analysis

Powder x-ray diffraction data was collected using microcrystalline samples on a Rigaku Ultima IV diffractometer (40 kV, 40 mA, CuKα1, 2 λ = 1.5418 Å). The measured parameter included a scan speed of 2(°)/min, a step size of 0.02(°).

Single Crystal X-ray diffraction structure analysis.

After supercritical carbon dioxide treatment, **NKMOF-1-Cu** crystals (cubic crystals of side length ~0.2 μm) were quickly loaded into the test sample tube and degassed for 3 hours at the degassing station. Then we used a pre-filled propyne or propadiene balloon as a gas source to fill the sample tube for 1 h. Subsequently, the single crystal was quickly transferred into Paratone-N oil, then mounted via a loop, and quickly

transferred to diffractometer. Finally, Single crystal diffraction data of **NKMOF-1-Cu**, **propyne@NKMOF-1-Cu** and **propadiene@NKMOF-1-Cu** was collected at 120 K via an Oxford Cryo stream system on a SuperNova (Mo) X-ray Source with micro-focus sealed X-ray tube. The structures were solved and refined using Olex2 with 'XS' and 'XL' plug-in. In order to fully display the propyne or propadiene molecules in an asymmetric unit, the structure of **propyne@NKMOF-1-Cu** and **propadiene@NKMOF-1-Cu** were solved in P-1 space group. CCDC number for **propyne @NKMOF-1-Cu** and **propadiene@NKMOF-1-Cu** are 1859293 and 1904988, respectively. We also tried to obtain the crystal structure of **NKMOF-1-Cu** capturing propylene. Unfortunately, we cannot observe propylene molecules in single crystal structure possibly due to low loading and relatively weak binding affinity of propylene.

Synthesis of NKMOF-1-Ni

NKMOF-1-Ni was synthesized according to a previously reported method[1]. Bulk purity of the sample was verified by PXRD (Figure S1). And it possesses excellent water stability (Figure S1 and Figure S2).

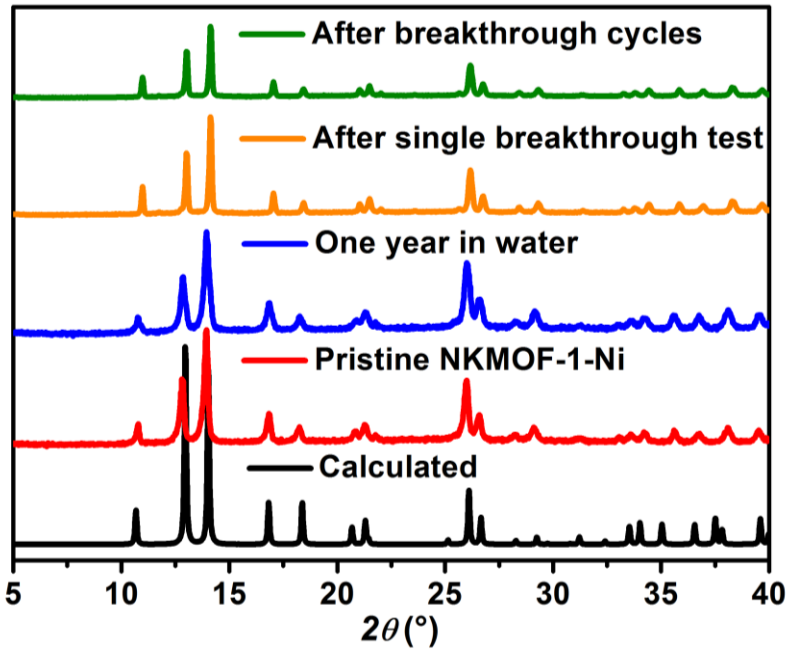

Figure S1. PXRD patterns of the calculated (black); pristine **NKMOF-1-Ni** (red);

NKMOF-1-Ni soaked in water for 1 year (blue); after breakthrough for first time (orange) and fifth time (green).

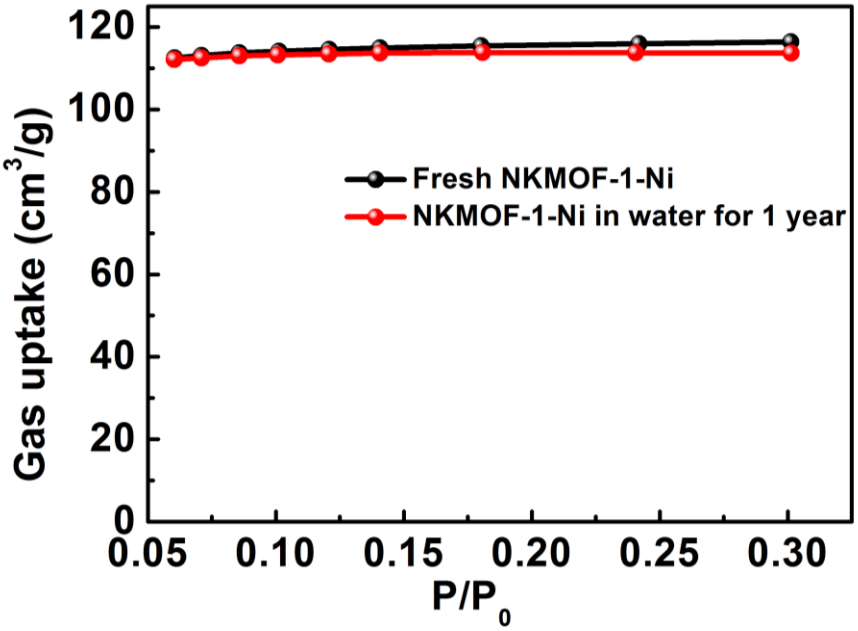

.

Figure S2. The adsorption isotherm of **NKMOF-1-Ni** in the particular P/P_0 range. Pristine **NKMOF-1-Ni** (black); **NKMOF-1-Ni** soaked in water for 1 year (red).

Synthesis of NKMOF-1-Cu

The powder and single crystal of **NKMOF-1-Cu** was prepared according to a previously reported method[1]. And it possesses excellent water stability (Figure S3)

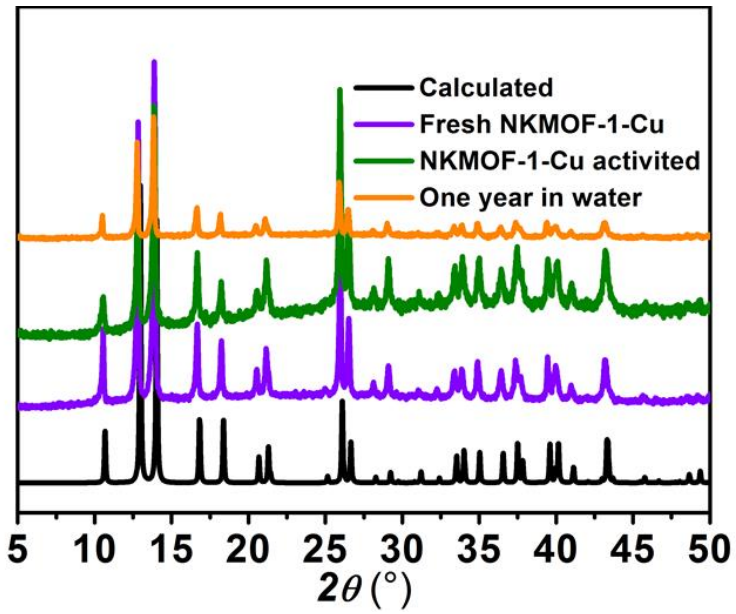

Figure S3. PXRD patterns of the calculated **NKMOF-1-Cu** (black); fresh **NKMOF-1-Cu** (purple); activated **NKMOF-1-Cu** (green) and **NKMOF-1-Cu** soaked in water for 1 year (orange).

Synthesis of ZU-62 (NbOFFIVE-2-Cu-i)

ZU-62 were prepared via previously reported procedure[2,3]. Bulk purity of the sample was verified by PXRD (Figure S24)

General procedure for activated of NKMOF-1-M. Powders of **NKMOF-1-Ni** was activated according to previously reported methods.[1] Single crystals sample of **NKMOF-1-Cu** was exchanged with methanol for one week, and the fresh methanol solvent was refreshed three times per day. Single-crystal sample was wrapped in paper in the invading state and quickly transferred to a sample pool of supercritical carbon dioxide activator filled with methanol. After that, the instrument is then switched on and exchanged with liquid carbon dioxide. During the operation, the temperature is controlled between 0 °C to 10 °C and fresh liquid carbon dioxide was exchanged every 2 hours. After two days of operation, the liquid carbon dioxide inlet valve and the outlet

valve are simultaneously opened for dynamic exchange for ~3 hours. In this process, it is required to keep the liquid level in the sample tank always higher than the sample. Then turn on the heating to make the sample tank in supercritical state (1072 psi, 31 °C) for 30 minutes, and finally discharge the gas in the sample tank in about 30 minutes. Subsequently, quickly load the sample into a sample tube pre-filled with argon for adsorption and Single crystal diffraction testing. The related adsorption data for **NKMOF-1-Cu** in this paper were tested according to this improved method.

Single component gas adsorption isotherm test. We used 200-250 mg of MOFs to test single component gas adsorption. **NKMOF-1-Ni** were evacuated at 90 ℃ for 10 h under dynamic pressure below 5 μm Hg. The single crystals sample of **NKMOF-1-Cu** was exchanged with methanol for one week, then were activated using carbon dioxide supercritical activator for two days as described in the section of **General procedure for activated of NKMOF-1-Cu**. After that, the sample was degassed at room temperature until the pressure dropped below 4 μm Hg. **ZU-62** were activated according to previous literature[3]. Single-component gas sorption isotherms were measured at 273K, 288K, 298K, 308K and 318K using ASAP 2020 PLUS Analyzer (Micromeritics) (Figure S4). For propyne, propadiene and propylene, their saturation adsorption was collected at different temperatures which are according to their boiling point temperatures (e.g. 253K for propyne, 231 K for propylene, 243 K for propadiene).

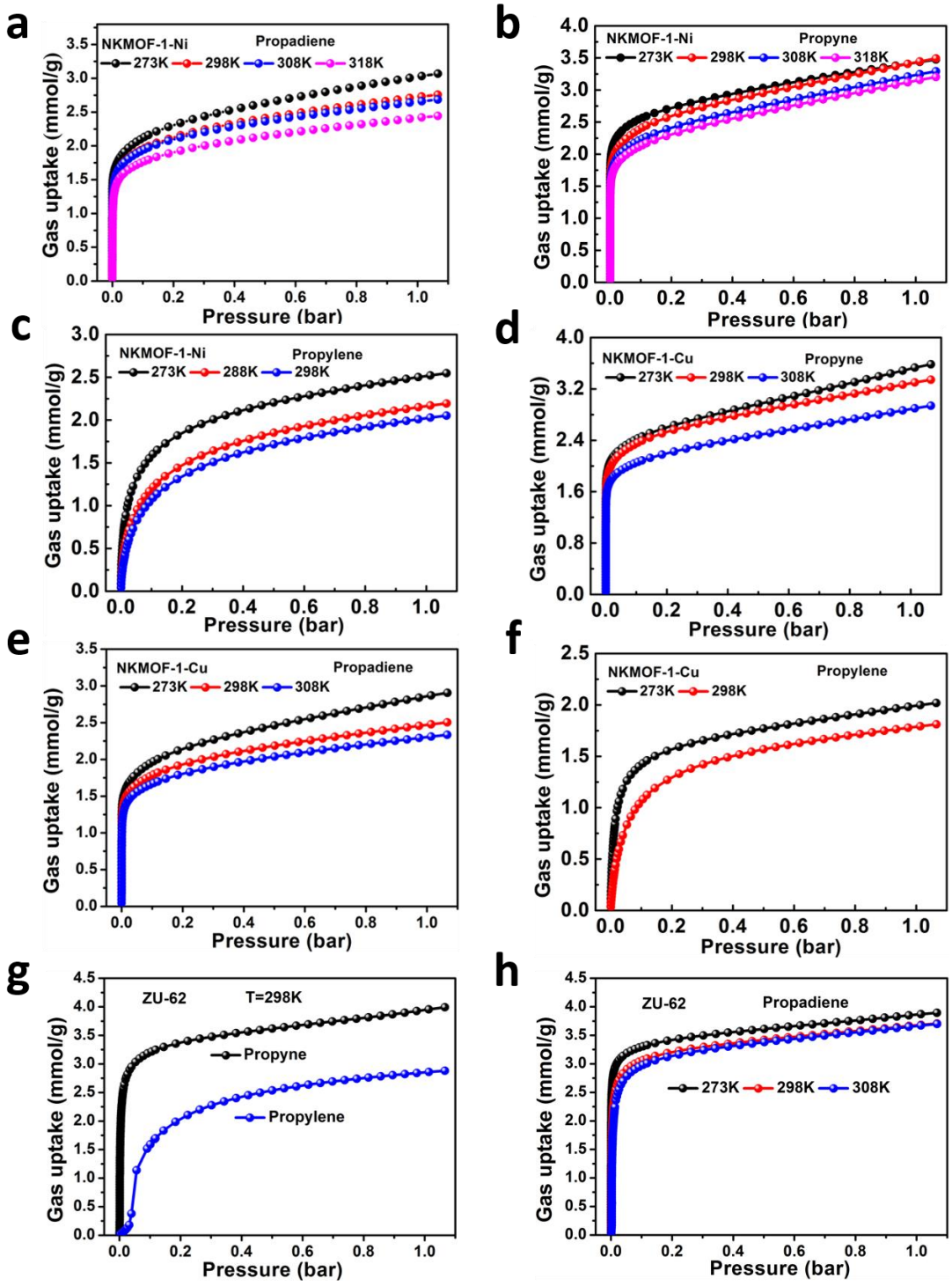

Figure S4. The schematic of various gas adsorption isotherms. (a, b, and c) Propadiene, propyne and propylene for **NKMOF-1-Ni**; (d, e and f) Propyne, propadiene, and propylene for **NKMOF-1-Cu**; (g, h) Propyne, propylene and propadiene for **ZU-62**.

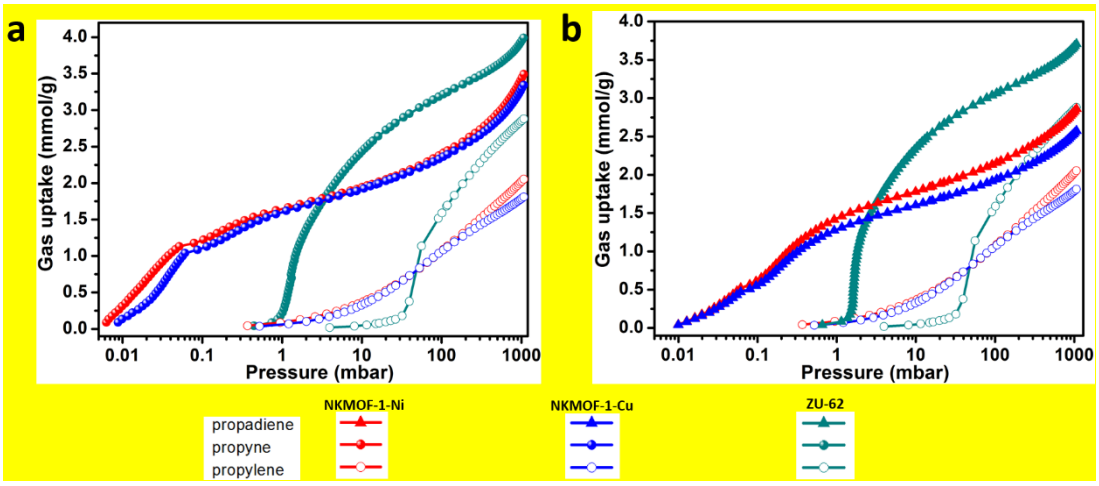

Figure S5. (a) Single-component (propyne and propylene) gas adsorption isotherm of **NKMOF-1-M** and **ZU-62** material at 298K (0-5mbar); (b) Single-component (propadiene and propylene) gas adsorption isotherms of **NKMOF-1-M** and **ZU-62** material at 298K (0-5mbar).

Fitting of single component adsorption isotherm and isosteric heat of adsorption (Q_{st})

The experimental isosteric heat of adsorption (Q_{st}) values for various gases in **NKMOF-1-M (M = Ni, Cu)** were determined by first fitting the adsorption isotherms at 273 K, 298 K, 308 K and 318 K for the respective adsorbates to the dual-site Langmuir-Freundlich (DSLF) equation[4], subsequently applying the Clausius-Clapeyron method[5]. The DSLF equation is given by:

$$n = \frac{n_{m1} b_1 P^{\left(\frac{1}{t_1}\right)}}{1+b_1 P^{\left(\frac{1}{t_1}\right)}} + \frac{n_{m2} b_2 P^{\left(\frac{1}{t_2}\right)}}{1+b_2 P^{\left(\frac{1}{t_2}\right)}} \quad \text{(DSLF)} \qquad (1)$$

where n is the uptake (in mmol g^{-1}), P is the pressure (in kPa), n_{m1} and n_{m2} are the saturation uptakes (in mmol g^{-1}) for sites 1 and 2, b_1 and b_2 are the affinity coefficients (in kPa^{-1}) for sites 1 and 2, and t_1 and t_2 represent the deviations from the ideal homogeneous surface (unit less) for sites 1 and 2. The parameters that were obtained

from the fitting of the propyne, propadiene and propylene adsorption isotherms are found in Table S1-S6 respectively.

The fitted parameters were used to calculate the Q_{st} values for a range of uptakes through the Clausius-Clapeyron equation, which is the following:

$$Q_{\mathrm{st}} = -R\frac{\partial \ln P}{\partial(1/T)} \tag{2}$$

Where T is the temperature (in K) and R is the ideal gas constant. The partial derivative term actually represents the slope of the plot of ln P *vs.* $1/T$ for a number of isotherms at different temperatures at various loadings. Therefore, the above Q_{st} equation can be simplified to:

$$Q_{\mathrm{st}} = -mR \tag{3}$$

where m is the slope, which can be calculated by the following for x (2 or 3)different temperatures and their corresponding pressures:

$$m = \frac{\Sigma\frac{1}{T_i}\ln P_i - \frac{1}{x}\left(\Sigma\frac{1}{T_i}\right)(\Sigma \ln P_i)}{\Sigma\left(\frac{1}{T_i}\right)^2 - \frac{1}{x}\left(\Sigma\frac{1}{T_i}\right)^2} \tag{4}$$

The P_i values were back-calculated for a range of uptakes using the DSLF equation *via* an iterative technique (e.g., the Newton–Raphson method)[6].

The experimental propyne, propadiene and propylene Q_{st} for **NKMOF-1-Ni** were also determined through a simultaneous fitting to the DSLF equation[7], Notably, b_1 and b_2 are expressed as a function of temperature via the following:

$$b_1 = b_{01}e^{\left(\frac{E1}{RT}\right)} \tag{5}$$

$$b_2 = b_{02}e^{\left(\frac{E2}{RT}\right)} \tag{6}$$

where R is the ideal gas constant, b_{01} and E_1 are the pre-exponential factor (in kPa^{-1}) and the activation energy (in kJ mol^{-1}) for site 1, and b_{02} and E_2 are analogous

parameters for site 2. The parameters obtained for the simultaneous fitting of the experimental propyne, propadiene and propylene adsorption isotherms at 298 K and 308 K in **NKMOF-1-Ni** are provided in Table S7-S11. These parameters were used to calculate the Q_{st} values for a range of uptakes using the following form of the Clausius-Clapeyron equation:

$$Q_{st} = \frac{-RT_1T_2}{T_2-T_1} \ln\left(\frac{P_1}{P_2}\right) \quad (7)$$

We note that it was very difficult to obtain the Q_{st} for propyne in both **NKMOF-1-M** materials through empirical fitting methods since they exhibit exceptionally high uptake for this adsorbate at low loadings. However, the Q_{st} curve that is shown for propyne in both MOFs in **Figure S6** should provide some approximation of the Q_{st} value corresponding to the adsorption of propyne at the primary binding site in the two materials. Indeed, the zero-coverage propyne Q_{st} values for both MOFs (**NKMOF-1-Ni** = 65.1 kJ mol^{-1}; **NKMOF-1-Cu** = 67.2 kJ mol^{-1}) are actually close to the corresponding DFT-calculated adsorption energies for this adsorbate about the four neighboring pyrazine units (**NKMOF-1-Ni** = 72.3 kJ mol^{-1}; **NKMOF-1-Cu** = 71.3 kJ mol^{-1}, see **Table S13-S14**). The Q_{st} curve that is shown suggests that the propyne molecules first adsorbs at site I, followed by binding at site II as reflected by the decrease in Q_{st} values after the initial loading. The Q_{st} value remains constant until about 1.25 mmol g^{-1} loading, at which the Q_{st} increases to a quantity that is near the zero-coverage value (representative of site I). A possible explanation for this is that the

propyne molecules could remain adsorbed at site II (due to strong interactions with the open-metal sites) and that the addition of more propyne molecules is required to push the site II-adsorbed molecules down the one-dimensional channels into site I.

The Q_{st} curve for propadiene in **NKMOF-1-Ni** (**Figure S7**) shows that the Q_{st} slightly increases to about 58 kJ mol^{-1} at roughly 1 mmol g^{-1} loading before sharply declining to a value of 25 kJ mol^{-1} at an uptake of 1.7 mmol g^{-1}. The increase that is observed before the drop in the Q_{st} plot could be due to both favorable MOF–propadiene and propadiene–propadiene interactions. Notably, all three carbon atoms of the propadiene molecule possess a *p* orbital, which makes π–π interactions possible between the terminal C atoms of neighboring propadiene molecules. Q_{st} values before and after the drop in the curve could probably be attributed to binding at sites I and II, respectively. The same two regions are also observed in the Q_{st} plot for propadiene in **NKMOF-1-Cu**.

Table S1. The fitted parameters for the DSLF equation for the propyne adsorption isotherms for **NKMOF-1-Ni** at 298 K, 308 K, and 318 K. R^2 values are provided.

Parameter	**298 K**	**308 K**	**318 K**
n_{m1} (mmol g^{-1})	25.0000	5570.2107	1989.4890
b_1 (kPa^{-1})	0.005.1782E-3	6.1494E-05	1.0307 E-04
t_1	4.0000	2.8524	2.2745
n_{m2} (mmol g^{-1})	1.2000	1.4459	1.5415
b_2 (kPa^{-1})	0.2263	301.6486	71.8939

t_2	0.5882	0.9412	1.0722
R^2	0.9969	0.9980	0.9984

Table S2. The fitted parameters for the DSLF equation for the propadiene adsorption isotherms for **NKMOF-1-Ni** at 273 K, 298 K, and 308 K. R^2 values are provided.

Parameter	**273 K**	**298 K**	**308 K**
n_{m1} (mmol g^{-1})	1.1601	1.3700	1.2997
b_1 (kPa^{-1})	8093.0430	54.5488	29.3408
t_1	0.6983	1.0488	0.9979
n_{m2} (mmol g^{-1})	1672.67624	30.9015	9.4708
b_2 (kPa^{-1})	0.00030	0.0096	0.0308
t_2	3.5648	2.8470	2.7527
R^2	0.9991	0.9997	0.9998

Table S3. The fitted parameters for the DSLF equation for propylene adsorption isotherms for **NKMOF-1-Ni** at 273 K, 288 K and 298 K. R^2 values are provided.

Parameter	**273 K**	**288 K**	**298 K**
n_{m1} (mmol g^{-1})	7.6073	3.9170	0.7000
b_1 (kPa^{-1})	5.5290E-03	1.2700E-03	1.0170E-3
t_1	1.6232	1.0862	1
n_{m2} (mmol g^{-1})	2.0398	2.2526	1.9

b_2 (kPa^{-1})	0.5129	0.2464	2.4493E-05
t_2	1.5646	1.5918	1
R^2	0.9999	0.9999	0.9999

Table S4. The fitted parameters for the DSLF equation for the propyne adsorption isotherms for **NKMOF-1-Cu** at 298 K and 308 K. R^2 values are also provided.

Parameter	**298 K**	**308 K**
n_{m1} (mmol g^{-1})	16.2759	4622.2281
b_1 (kPa^{-1})	3.92E-2	4.1635E-05
t_1	3.6728	2.3993
n_{m2} (mmol g^{-1})	1.2442	1.5335
b_2 (kPa^{-1})	11188.0949	72.3994
t_2	0.5858	1.0509
R^2	0.9965	0.9980

Table S5. The fitted parameters for the DSLF equation for the propadiene adsorption isotherms for **NKMOF-1-Cu** at 273 K, 298 K, and 308 K. R^2 values are provided.

Parameter	**273 K**	**298 K**	**308 K**
n_{m1} (mmol g^{-1})	10445.6439	6858.7471	6473.5439
b_1 (kPa^{-1})	3.9919E-05	3.5937E-05	3.3805E-5

t_1	3.2869	2.8698	2.8167
n_{m2} (mmol g^{-1})	1.1173	1.2275	1.1659
b_2 (kPa^{-1})	7.20E+03	4.80E+01	3.08E+01
t_2	0.7120	1.0683	0.9976
R^2	0.9990	0.9997	0.9999

Table S6. The fitted parameters for the DSLF equation for the propylene adsorption isotherms for **NKMOF-1-Cu** at 273 K and 298 K. R^2 values are also provided.

Parameter	**273 K**	**298 K**
n_{m1} (mmol g^{-1})	31.5771	1.2000
b_1 (kPa^{-1})	4.6400E-04	0.000344211
t_1	1.3151	1.000
n_{m2} (mmol g^{-1})	1.5419	1.000
b_2 (kPa^{-1})	0.8519	1.5592E-05
t_2	1.1303	1.0000
R^2	0.9999	0.9999

Table S7. DSLF parameter fits for propyne in **NKMOF-1-Ni** as obtained through simultaneous fitting of the adsorption isotherms at 308 K and 318 K.

	Site 1				Site 2				
	n_{m1}	b_{01}	E_1	t_1	n_{m2}	b_{02}	E_2	t_2	R^2
NKMOF-1-Ni	1.32901	1.1037E-08	60.2618	1.0284	13.6167	2.56E-6	2.9001	23.8315	0.9970

Table S8. DSLF parameter fits for propylene in **NKMOF-1-Ni** as obtained through simultaneous fitting of the adsorption isotherms at 298 K and 308 K

	Site 1				Site 2				
	n_{m1}	b_{01}	E_1	t_1	n_{m2}	b_{02}	E_2	t_2	R^2
NKMOF-1-Ni	4.2789	2.4300E-07	20.3363	1.1019	2.2737	1.0800 E-05	24.2281	1.5704	0.9999

Table S9. DSLF parameter fits for propyne in **NKMOF-1-Cu** as obtained through simultaneous fitting of the adsorption isotherms at 298 K and 308 K.

	Site 1				Site 2				
	n_{m1}	b_{01}	E_1	t_1	n_{m2}	b_{02}	E_2	t_2	R^2
NKMOF-1-Cu	1.5101	2.5290E-08	58.1572	1.02189	39.8038	4.5199E-4	6.9346	2.4576	0.9979

Table S10. DSLF parameter fits for propadiene in **NKMOF-1-Cu** as obtained through simultaneous fitting of the adsorption isotherms at 273 K and 298 K.

	Site 1				Site 2				
	n_{m1}	b_{01}	E_1	t_1	n_{m2}	b_{02}	E_2	t_2	R^2
NKMOF-1-Cu	8.9477	7.3516E-04	8.0647	2.2476	1.3326	1.68E-6	41.9953	1.1411	0.9975

Table S11. DSLF parameter fits for propylene in **NKMOF-1-Cu** as obtained through simultaneous fitting of the adsorption isotherms at 298 K and 308 K

	Site 1				Site 2				
	n_{m1}	b_{01}	E_1	t_1	n_{m2}	b_{02}	E_2	t_2	R^2

NKMOF-1-Cu	1.5970	4.9500E-07	32.5238	1.1464	1.1412	8.6300E-06	13.2464	0.8718	0.9999

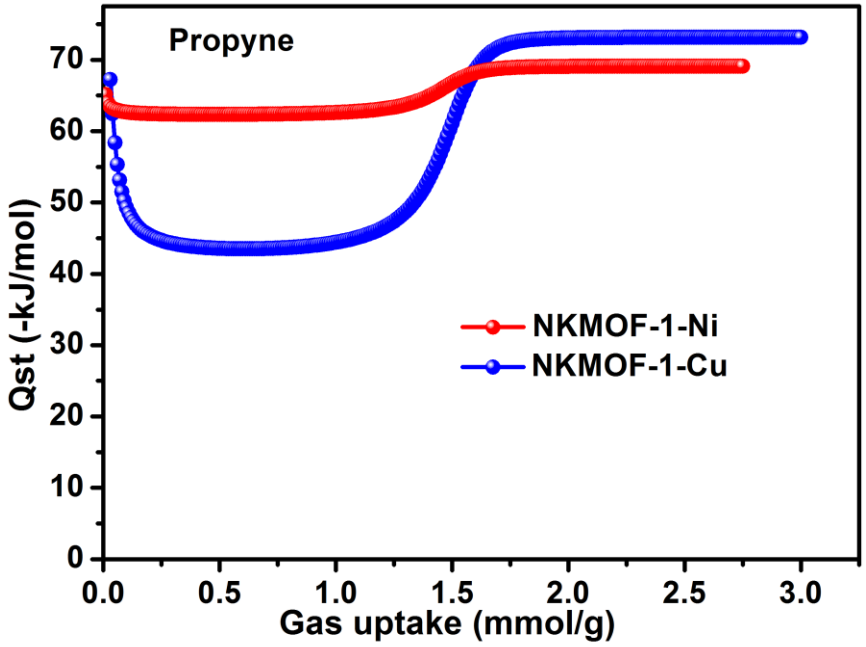

Figure S6. Q_{st} curves of propyne for **NKMOF-1-Ni** and **NKMOF-1-Cu**.

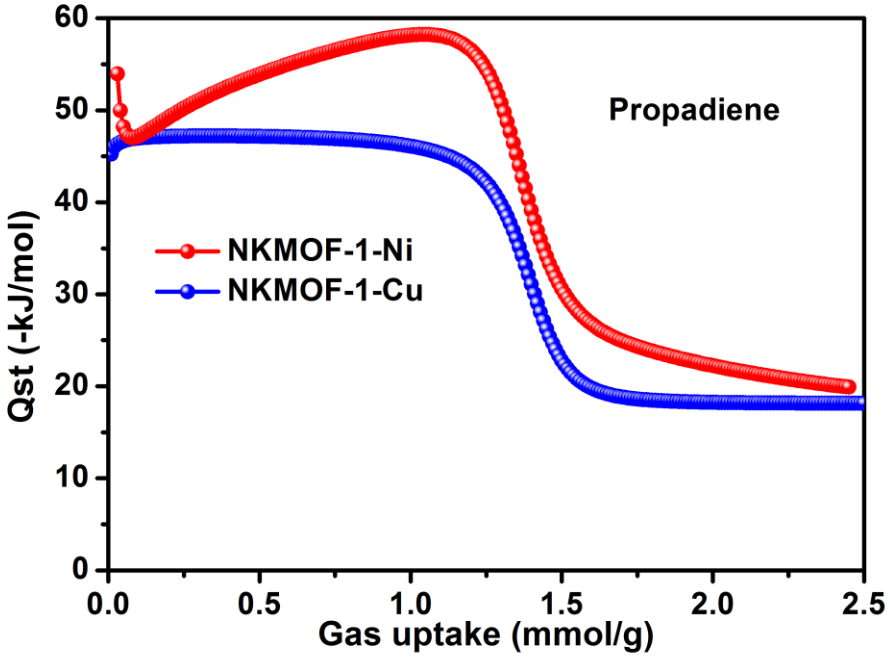

Figure S7. Q_{st} curves of propadiene for **NKMOF-1-Ni** and **NKMOF-1-Cu**.

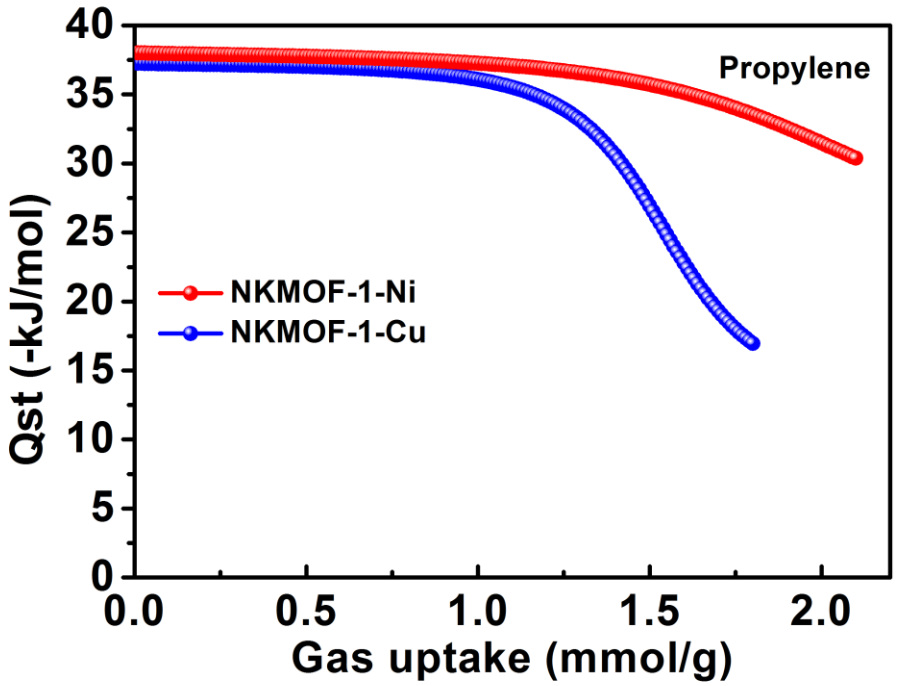

Figure S8. Q_{st} curves of propylene for **NKMOF-1-Ni** and **NKMOF-1-Cu**.

Table S12. Comparison of surface areas, IAST selectivity for propadiene/propyne/propylene (0.5/0.5/99) mixture for ternary mixture (298 K) and simulated breakthrough propylene productivity (propadiene+pyopyne<40ppm, at 298 K) for various benchmarking ultramicroporous MOFs.

	S_{BET} (m^2/g)	propadiene/propylene selectivities (1 ~ 100kPa)	propyne/propylene selectivities (1 ~ 100kPa)	propylene productivity at 1bar (mol/L)
NKMOF-1-Ni	382	127.5~236.5	630.4~1217.8	191.1
NKMOF-1-Cu	374	100.8~193.4	610.5~859.5	163.3

ZU-62	476	11.5~30.0	21.3~38.9	70.6

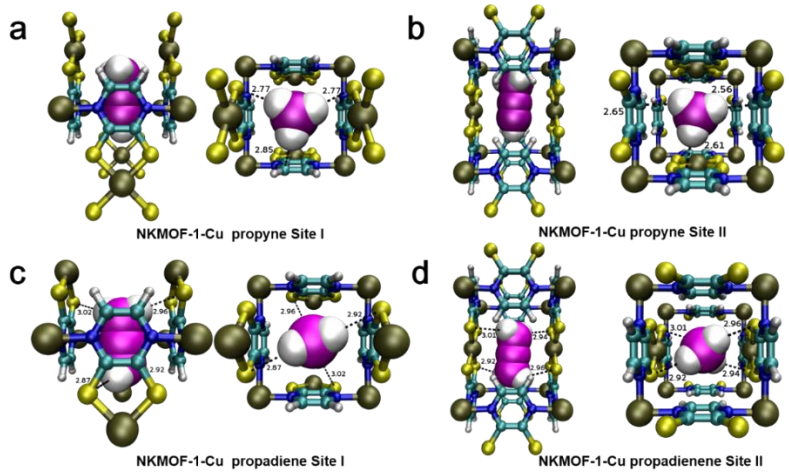

Figure S9. Two binding sites (I, II) of propyne and propadiene determined by modelling studies conducted upon **NKMOF-1-Cu.** (a) Site I for propyne; (b) site II for propyne; (c) Site I for propadiene; (d) Site II for propadiene. Atom colors: C (MOF) = teal, C (propyne and propadiene) = pink, H = white, N = blue, S = yellow, Cu = gold.

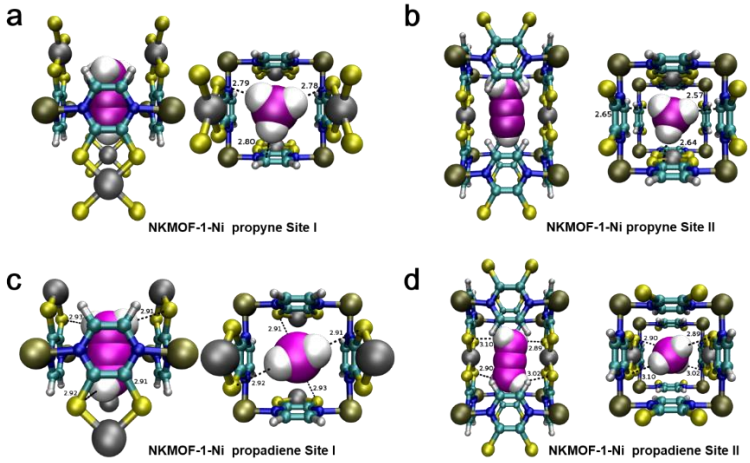

Figure S10. Perspective views (left = a/b-axis, right = c-axis) of a portion of the crystal structure of **NKMOF-1-Ni** showing the optimized position of a propyne and propadiene molecule about (a, c) the pyrazine units and (b, d) the NiS_4 units in the MOF as determined through periodic DFT calculations using VASP. The closest MOF–

propyne distances are also shown in the *c*-axis views. Atom colors: C(MOF) = teal, C(propyne) = pink, H = white, N = blue, S = yellow, Cu = gold, Ni = lavender.

Table S13. Calculated adsorption energies (in kJ mol^{-1}) for a single propyne, propadiene and propylene molecule at two sites in **NKMOF-1-Ni** as determined from periodic DFT calculations using VASP. Site I corresponds to adsorption between the pyrazine units and site II is between the NiS_4 units.

Adsorbate	**Site**	**ΔE (kJ mol^{-1})**
propyne	I	-72.3
	II	-47.2
propadiene	I	-68.1
	II	-43.7
propylene	I	-59.0
	II	-49.6

Table S14. Calculated adsorption energies (in kJ mol^{-1}) for a single propyne, propadiene and propylene molecule at two sites in **NKMOF-1-Cu** as determined from periodic DFT calculations using VASP. Site I corresponds to adsorption between the pyrazine units and site II is between the CuS_4 units.

Adsorbate	**Site**	**ΔE (kJ mol^{-1})**
propyne	I	-71.3
	II	-51.1
propadiene	I	-64.5

	II	-48.2
propylene	I	-57.0
	II	-53.2

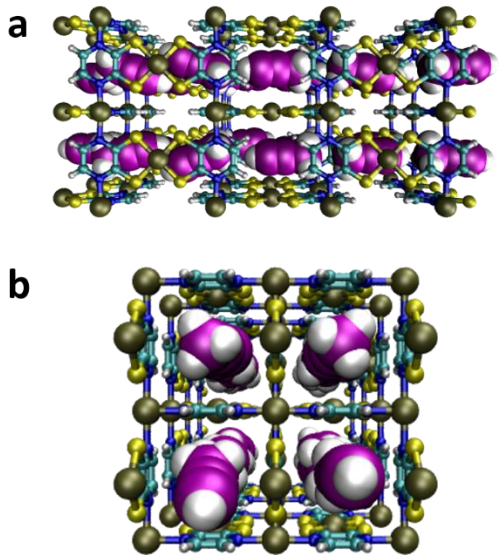

Figure S11. (a) Perspective *a/b*-axis view and (b) *c*-axis view of the modeled 3 × 3 × 2 supercell in **NKMOF-1-Cu** at propyne saturation. Atom colors: C(MOF) = teal, C(propyne) = pink, H = white, N = blue, S = yellow, Cu = gold.

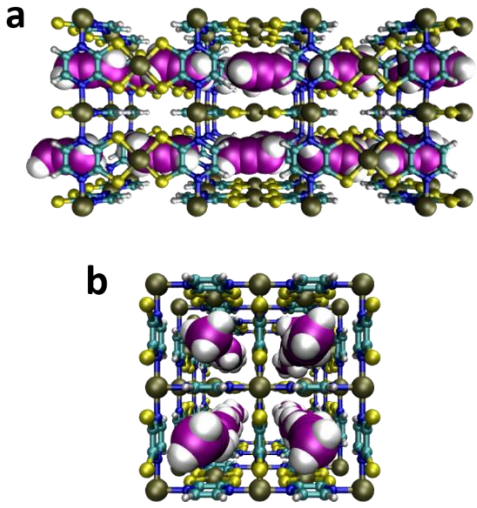

Figure S12. (a) Perspective *a/b*-axis view and (b) *c*-axis view of the modeled 3 × 3 × 2 supercell in **NKMOF-1-Cu** at propadiene saturation. Atom colors: C(MOF) = teal,

C(propadiene) = pink, H = white, N = blue, S = yellow, Cu = gold.

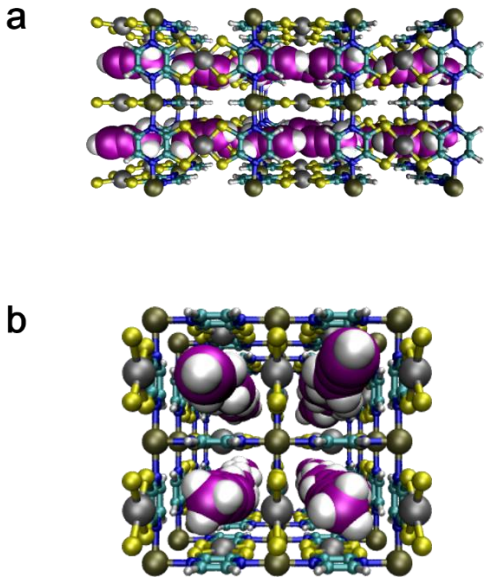

Figure S13. (a) Perspective *a/b*-axis view and (b) *c*-axis view of the modeled 3 × 3 × 2 supercell in **NKMOF-1-Ni** at propyne saturation. Atom colors: C(MOF) = teal, C(propyne) = pink, H = white, N = blue, S = yellow, Cu = gold, Ni = lavender.

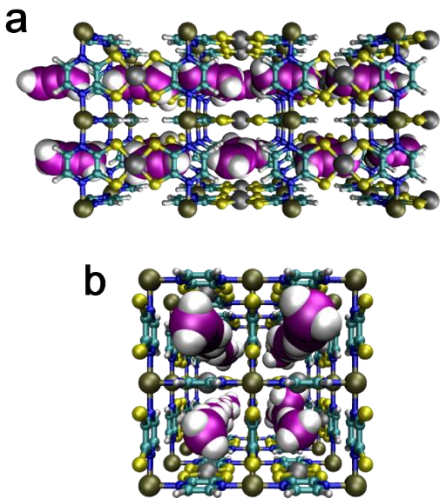

Figure S14. (a) Perspective *a/b*-axis view and (b) *c*-axis view of the modeled 3 × 3 × 2 supercell in **NKMOF-1-Ni** at propadiene saturation. Atom colors: C(MOF) = teal, C(propadiene) = pink, H = white, N = blue, S = yellow, Cu = gold, Ni = lavender.

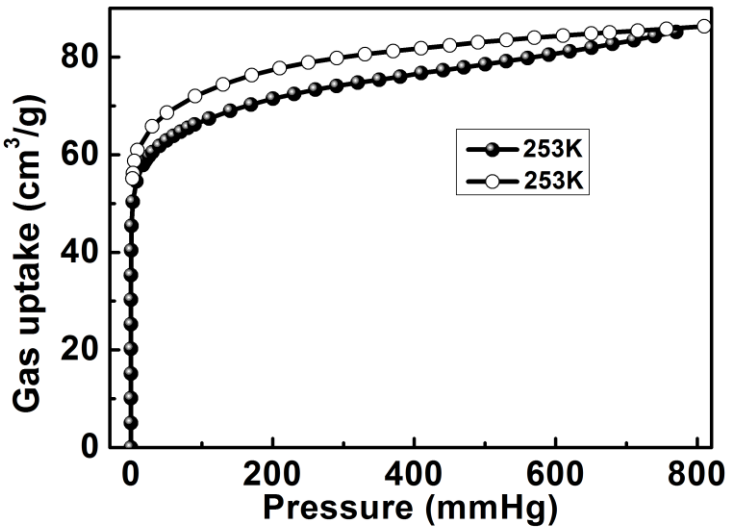

Figure S15. The schematic of propyne gas adsorption isotherm for **NKMOF-1-Ni** at 253 K.

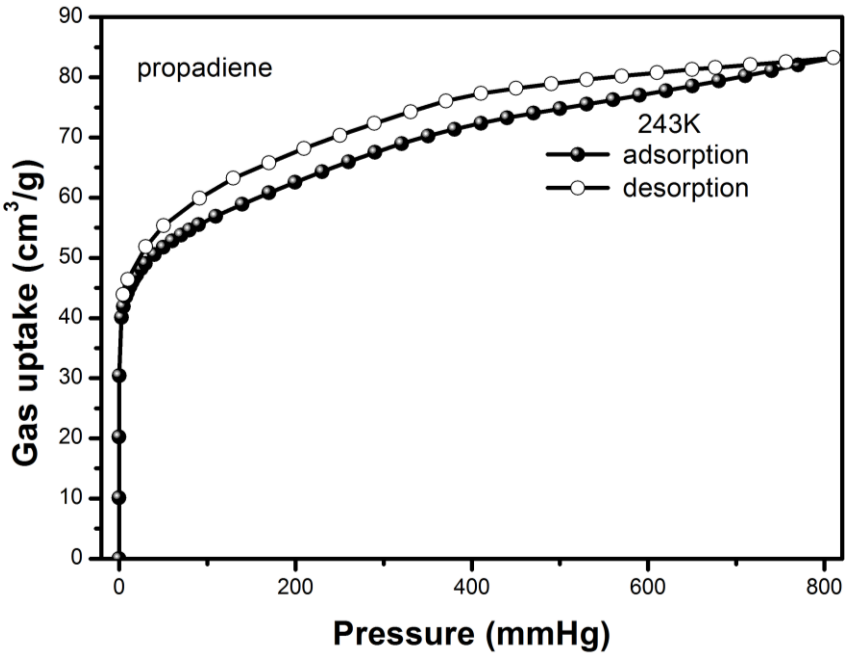

Figure S16. The schematic of propadiene gas adsorption isotherm for **NKMOF-1-Ni** at 243 K.

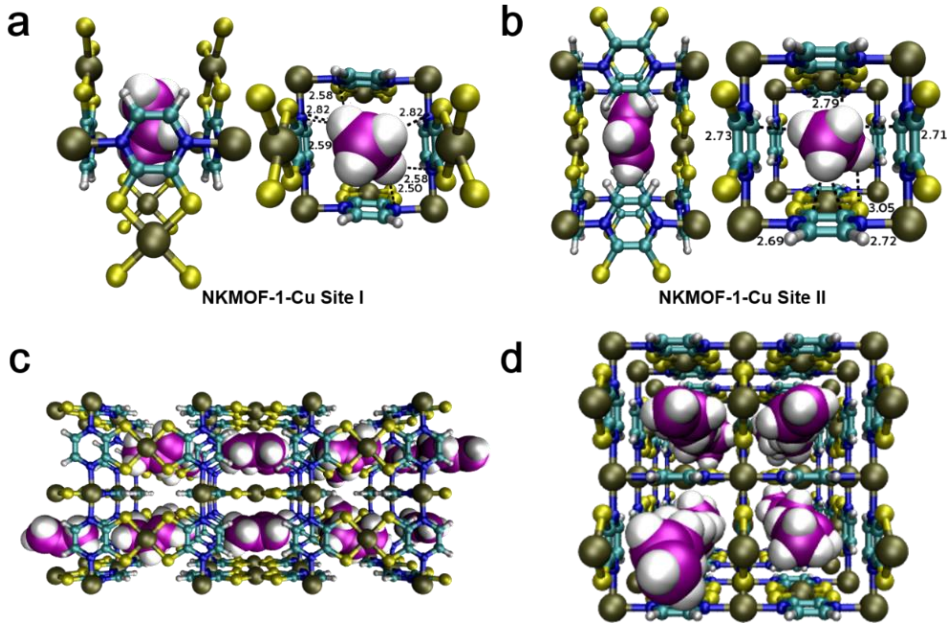

Figure S17. Perspective views (left = a/b-axis, right = c-axis) of a portion of the crystal structure of **NKMOF-1-Cu** showing the optimized position of a propylene molecule: (a) the pyrazine units and (b) the NiS_4 units in the MOF as determined through periodic DFT calculations using VASP. (c) Perspective *a/b*-axis view and (d) *c*-axis view of the modeled 3 × 3 × 2 supercell in **NKMOF-1-Cu** at propylene saturation The closest MOF–propylene distances are also shown in the *c*-axis views. Atom colors: C(MOF) = teal, C(propylene) = pink, H = white, N = blue, S = yellow, Cu = gold.

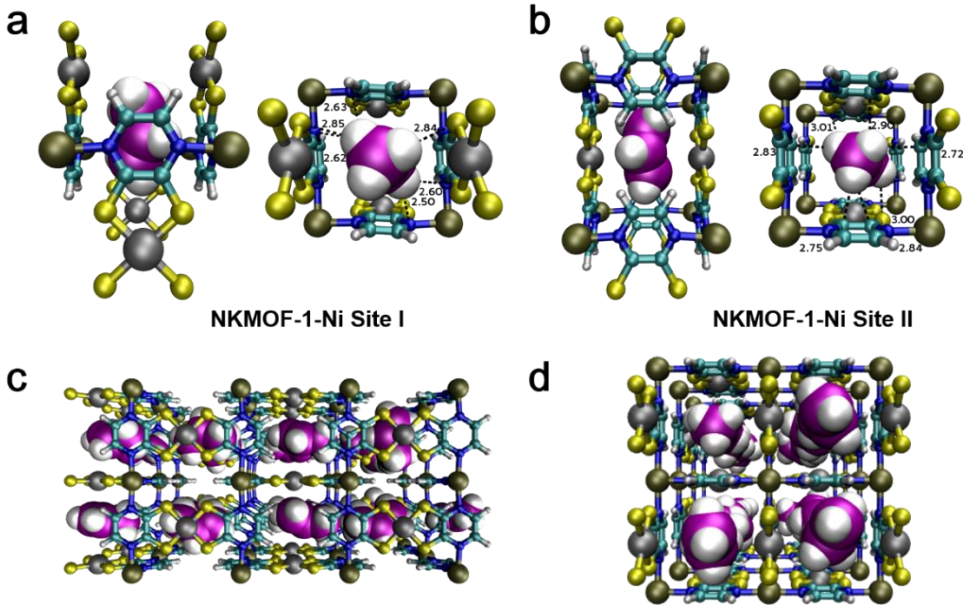

Figure S18. Perspective views (left = a/b-axis, right = c-axis) of a portion of the crystal structure of **NKMOF-1-Ni** showing the optimized position of a propylene molecule: (a) the pyrazine units and (b) the NiS_4 units in the MOF as determined through periodic DFT calculations using VASP. (c) Perspective *a*/*b*-axis view and (d) *c*-axis view of the modeled 3 × 3 × 2 supercell in **NKMOF-1-Ni** at propylene saturation. The closest MOF–propylene distances are also shown in the *c*-axis views. Atom colors: C(MOF) = teal, C(propylene) = pink, H = white, N = blue, S = yellow, Cu = gold, Ni = lavender.

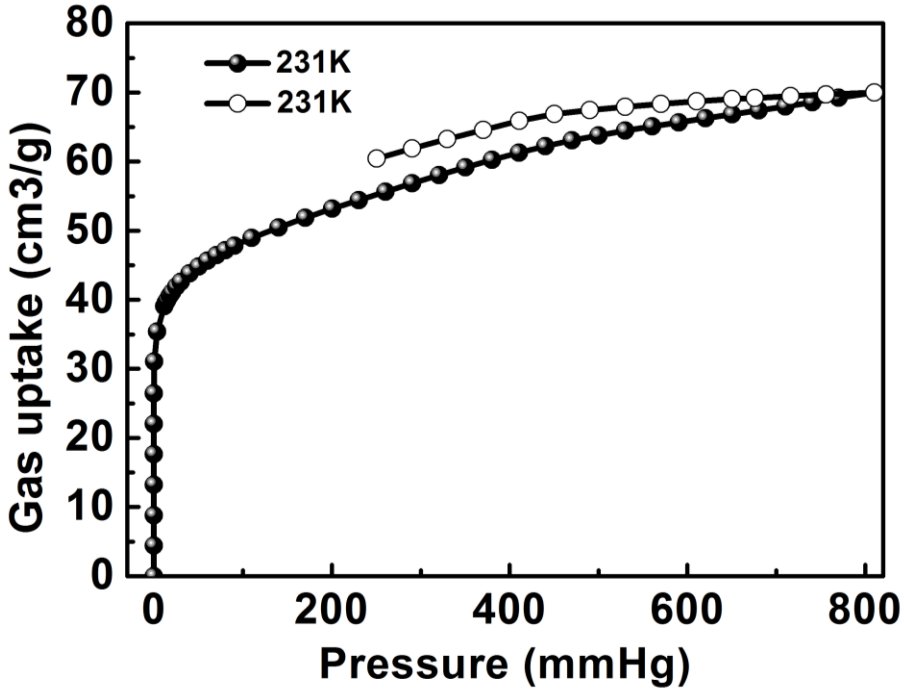

Figure S19. The schematic of propylene gas adsorption isotherm for **NKMOF-1-Ni** at 231 K.

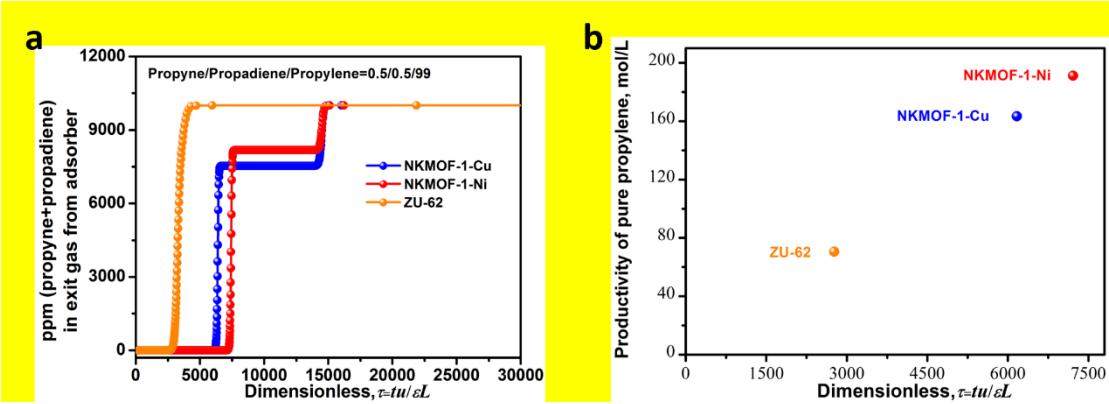

Figure S20. (a) Simulation breakthrough curves of ternary mixture (propadiene/propyne/propylene); (b) Productivity of pure propylene (propyne+propadiene < 40 ppm) at 298 K.

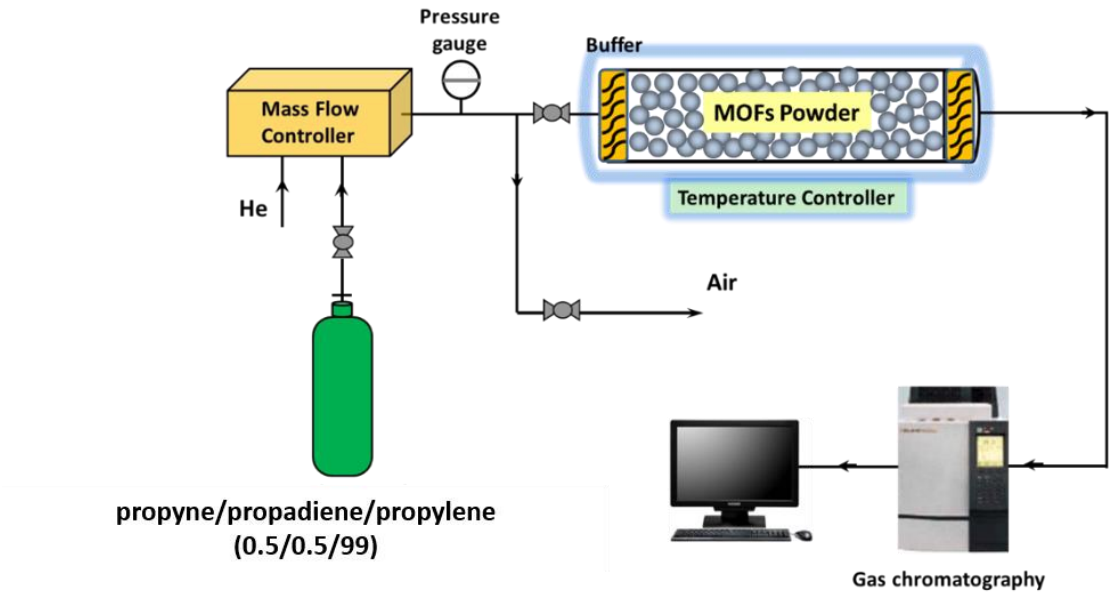

Scheme S1. Breakthrough separation apparatus.

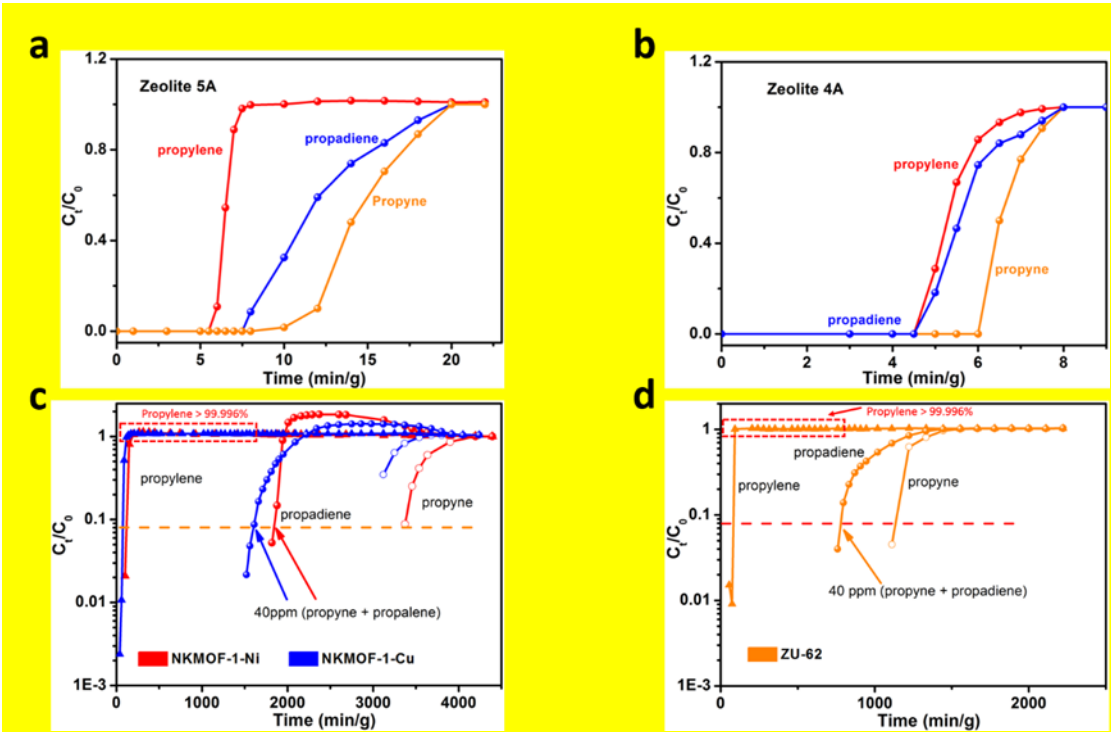

Figure S21. Propyne/propadiene/propylene (0.5/0.5/99) mixture breakthrough curves. (a) **Zeolite 5A**; (b) **Zeolite 4A**. Gas: propyne = empty circle, propadiene = solid circle, propyne = tringle. (c) The concentrations of propylene in breakthrough experiments of **NKMOF-1-Ni** and **NKMOF-1-Cu** for propyne/propadiene/propylene (0.5/0.5/99, v/v/v). (d) The concentrations of propylene in breakthrough experiments of **ZU-62** for

propyne/propadiene/propylene (0.5/0.5/99, v/v/v).

Table S15. Comparisons of propylene productivities in a single breakthrough operation using propadiene/propyne/propylene (0.5/0.5/99) mixture as input.

	Crystal density (g/cm^3)	Sample weight (g)	Gravimetric/Volumetric productivity (mmol/g and mol/L) of pure propylene (propadiene+propyne < 40 ppm)
NKMOF-1-Ni	1.713	1.03	134/230
NKMOF-1-Cu	1.734	1.00	125/218
ZU-62	1.378	1.08	55/76
Zeolite 5A	1.58	1.20	0.25/0.4
Zeolite 4A	1.52	1.10	0.00/0.00

DFT Modeling Studies. Periodic density functional theory (DFT) calculations were performed to evaluate the adsorption energy (ΔE) for propyne, propadiene and propylene about two previously determined sites for other gases in **NKMOF-1-Ni** and **-Cu**: (I) between the pyrazine units and (II) between the MS_4 units[1]. These calculations were implemented with the Vienna *ab initio* Simulation Package (VASP)[8,9] with the projector augmented wave (PAW) method[10,11] and Perdew-Burke-Ernzerhof (PBE) functional[12]. Furthermore, dispersion effects were treated using the DFT-D2 correction method of Grimme[13].

For both sites, the position of a single molecule of each adsorbate was initially optimized within the rigid unit cell of the individual MOFs. Afterward, another optimization was carried out in which the position of all atoms and lattice parameters of the system were allowed to fluctuate. All optimizations were converged to within

10^{-6} eV. The optimized position of a propyne, propadiene and propylene molecule about both sites within **NKMOF-1-Cu** are displayed in Figure S9 and Figure S17a and S17b, respectively, while those for **NKMOF-1-Ni** are displayed in Figure S10 and Figure S18a and S18b, respectively. The ΔE for the adsorbates localized about the two binding sites in both MOFs were calculated by the following:

$\Delta E = E(\text{MOF + Adsorbate}) - E(\text{MOF}) - E(\text{Adsorbate})$

where E(MOF + Adsorbate) is the energy of the unit cell of the MOF with the adsorbate, E(MOF) is the energy of the empty unit cell, and E(Adsorbate) is the energy of the adsorbate. The calculated ΔE values for propyne, propadiene and propylene about both sites in **NKMOF-1-Ni** and **NKMOF-1-Cu** are listed in Table S13, S14, respectively.

Grand Canonical Monte Carlo

Classical simulations of propyne, propadiene, and propene adsorption were performed in **NKMOF-1-Ni** and **NKMOF-1-Cu** using grand canonical Monte Carlo (GCMC) methods[14] within a 3 × 3 × 2 supercell of the respective MOFs. The same force field parameters that were established previously for both MOFs[1] were used for the simulations in this work. A spherical cut-off distance of 10.3574 and 10.2333 Å was used for **NKMOF-1-Ni** and **NKMOF-1-Cu**, respectively; these values correspond to half the shortest system cell dimension length for the individual MOFs. propyne, propadiene, and propene were modeled using newly developed polarizable potentials of the respective adsorbates (see next subsection). The total potential energy of the MOF-adsorbate system was calculated through the sum of the repulsion/dispersion,

stationary electrostatic, and polarization energies. These were calculated using the Lennard-Jones 12–6 potential, partial charges with Ewald summation[15,16], and a Thole-Applequist type model[17-20], respectively. All MOF atoms were kept fixed throughout the simulations. All simulations were performed using the Massively Parallel Monte Carlo (MPMC) code[21]. According to the simulations, saturation of propyne, propadiene, and propene in both MOFs is achieved at 2.5, 2.5 and 2 molecules per unit cell, respectively. The saturated structure of propyne and propadiene in **NKMOF-1-M** contains 1.5 and 1 molecule per unit cell at sites I and II, respectively. On the other hand, there is 1 molecule at each site in the saturated structure of propylene in both MOFs. Propylene has a less favorable fit about the four adjacent pyrazine units due to the larger molecular dimensions of this molecule compared to propyne and propadiene as shown in Scheme 1. The modeled 3 × 3 × 2 system cell of **NKMOF-1-Cu** containing the saturated loading amount for propyne, propadiene, and propene are shown in Figure S11, S12 and S17c, respectively, while such modeled structures for **NKMOF-1-Ni** are given in Figure S13, S14 and S18c, respectively.

Propyne, Propadiene, and Propylene Potentials

Ab initio models for propyne, propadiene and propylene were developed by constraining most molecular properties and fitting the repulsion/dispersion parameters to reproduce coupled cluster quality single point energies in a least squares manner. The molecules were treated as rigid and their geometries fixed at the DLPNO-CCSD(T)/aug-cc-pVTZ level of theory. Point charges on the atom centered sites were obtained via a CHELPG fit[22,23] on a HF/aug-cc-pVQZ wavefunction in the case of

propyne and propene and on an orbital optimized CCSD/aug-cc-pVTZ density in the case of propadiene. Atomic polarizabilities were taken from the set of van Duijnen[24] for consistency with the MOF parameters and the total molecular polarizability for propyne and propylene and the total molecular polarizability for both molecules are within 20% of a CP-SCF calculation at the HF/aug-cc-pVTZ level of theory. Atomic polarizabilities for propadiene were obtained from via the default procedure in the CamCASP program on a PBE0/aug-cc-pVQZ density[25]. 300 random dimer configurations were generated each for propene–propene, propene–propyne, and propyne–propyne with center of mass distances between 0 and 10 Å. Unphysically repulsive configurations were filtered when atoms overlapped by less than 80% of their van der Waals distance. Single point interaction energies for each dimer configuration were calculating using a DLPNO-CCSD(T)/DLPNO-MP2 extrapolation for the correlation energy with the basis sets aug-cc-pVDZ/aug-cc-pVTZ for for propyne and propene dimers and a DLPNO-CCSD(T) extrapolation for the correlation energy with aug-cc-pVDZ/aug-cc-pVTZ for propadiene. Repulsion/dispersion parameters were then fit using simulated annealing in a least squares manner using the in-house Monte Carlo code MPMC.[21] All *ab initio* calculations were performed in the gas phase with the electronic structure code ORCA[26] unless otherwise specified. The parameters and XYZ atomic coordinates for the propyne, propadiene and propylene potentials used in this work are displayed in Table S16, S17 and S18, respectively.

It appears that the molecular dimensions and orientation of the propylene molecule provides for a less favorable fit between the four neighboring pyrazine rings (Figure

S17 and S18). Adsorption energies of -49.6 and -53.2 kJ mol^{-1} were calculated for propylene about site II in **NKMOF-1-Ni** and **-Cu**, respectively (Table S13 and S14). Interestingly, the adsorption energy for propylene at site II is slightly higher than that for propyne and propadiene about the same site in both MOFs. This could be due to the fact that propylene molecule contains more H atoms to interact with the proximal S atoms through hydrogen bonding when it is adsorbed between the open-metal sites (Figure S17 and S18). GCMC simulations indicate that saturation of propylene in **NKMOF-1-M** is achieved at 2.0 molecules per unit cell, which agrees with the experimental saturated adsorption data of **NKMOF-1-Ni** (~1.9 molecules per unit cell at 1 bar, Figure S19).

Table S16. Parameters and *XYZ* atomic coordinates (in Å) for the propyne potential utilized in this work. ε and σ represent Lennard-Jones 12-6 parameters, *q* represents the point partial charge, and α° corresponds to the static point polarizability.

Atom	*x*	*y*	*z*	ε (K)	σ (Å)	*q* (e^-)	α° ($Å^3$)
C	-0.496283	-0.087396	0.018611	59.44730	3.37409	0.27794	1.28860
C	-1.688096	-0.299038	0.060781	59.44730	3.37409	-0.68447	1.28860
C	0.946631	0.167831	-0.033934	59.44730	3.37409	-0.46702	1.28860
H	-2.734565	-0.485212	0.097659	1.68278	2.62802	0.38484	0.41380
H	1.457545	-0.349203	0.780465	1.68278	2.62802	0.16274	0.41380
H	1.150775	1.236404	0.055917	1.68278	2.62802	0.16290	0.41380
H	1.363972	-0.183395	-0.979511	1.68278	2.62802	0.16307	0.41380

Table S17. Parameters and *XYZ* atomic coordinates (in Å) for the propadiene potential utilized in this work. ε and σ represent Lennard-Jones 12-6 parameters, *q* represents the point partial charge, and α° corresponds to the static point polarizability.

Atom	x	y	Z	ε (K)	σ (Å)	q (e–)	α° (Å3)
C	1.020127	2.320511	2.132990	51.20132	3.24802	0.26728	1.52153
C	0.538533	3.511768	2.407564	56.12209	3.58956	-0.60635	1.52153
C	1.502260	1.129540	1.858156	56.12209	3.58956	-0.60635	1.52153
H	-0.317430	3.628322	3.062190	10.35030	2.10157	0.23636	0.28633
H	0.986677	4.403707	1.985193	10.35030	2.10157	0.23636	0.28633
H	1.137083	0.564076	1.008633	10.35030	2.10157	0.23636	0.28633
H	2.275514	0.686579	2.475138	10.35030	2.10157	0.23636	0.28633

Table S18 Parameters and *XYZ* atomic coordinates (in Å) for the propylene potential utilized in this work. ε and σ represent Lennard-Jones 12-6 parameters, *q* represents the point partial charge, and α° corresponds to the static point polarizability.

Atom	*x*	*y*	*z*	ε (K)	σ (Å)	*q* (e^-)	α° ($Å^3$)
C	1.279733	0.056186	0.297444	64.19993	3.49559	-0.68011	1.28860
C	-0.013299	0.395647	0.361412	64.19993	3.49559	0.11067	1.28860
C	-1.114477	-0.281193	-0.405369	64.19993	3.49559	-0.28026	1.28860
H	2.029743	0.582144	0.876144	1.35098	2.53718	0.22630	0.41380
H	1.618683	-0.758020	-0.335600	1.35098	2.53718	0.25870	0.41380

H	-0.307277	1.217654	1.010051	1.35098	2.53718	0.08851	0.41380
H	-0.720729	-1.086530	-1.029165	1.35098	2.53718	0.10142	0.41380
H	-1.859915	-0.703431	0.275203	1.35098	2.53718	0.08741	0.41380
H	-1.635579	0.432912	-1.050121	1.35098	2.53718	0.08735	0.41380

Simulated breakthrough of mixtures in fixed bed adsorbers

The performance of industrial fixed bed adsorbers is dictated by a combination of adsorption selectivity and uptake capacity. Transient breakthrough simulations were carried out for 0.5/0.5/99 propyne/propadiene/propylene mixtures operating at a total pressure of 100 kPa and 298 K, using the methodology described in earlier publications.[27-30] For the breakthrough simulations, the following parameter values were used: length of packed bed, L = 0.3 m; voidage of packed bed, ε = 0.4; superficial gas velocity at inlet, u = 0.04 m/s. The transient breakthrough simulation results are presented in terms of a *dimensionless* time, τ, defined by dividing the actual time, t, by the characteristic time, $\frac{L\varepsilon}{u}$.

For comparisons of the separation performance, we plot the ppm (propyne+propadiene) in the gaseous product mixture leaving the adsorber as a function of the dimensionless time, τ. The plots for all five MOFs are provided in Fig.5a. As illustration, the plot for NKMOF-1-Ni is shown in **Figure S22**

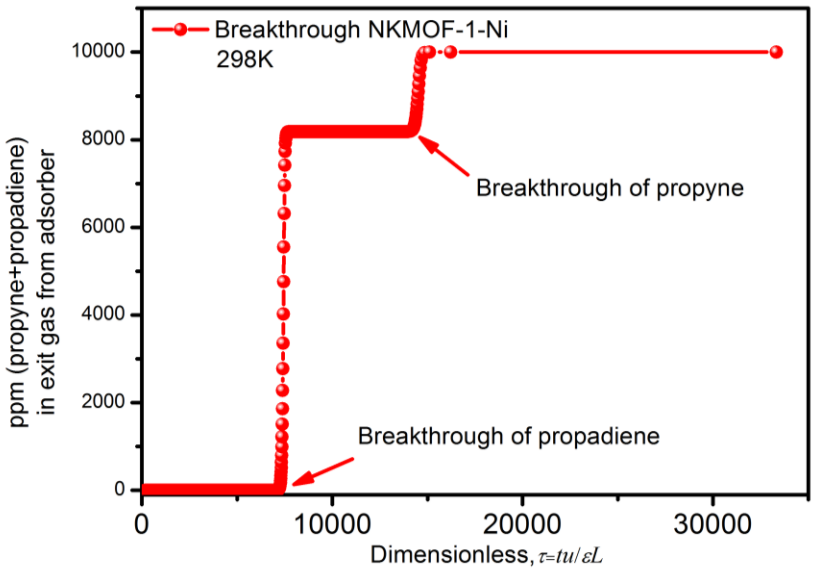

Figure S22. Simulation breakthrough curves of **NKMOF-1-Ni**

The plots show two distinct steps in the increase of the ppm (propyne+propadiene) impurity in the product propylene leaving the adsorber. The first step corresponds to the breakthrough of propadiene that is more poorly adsorbed than propyne. The second step corresponds to the breakthrough of propyne, the most strongly adsorbed component.

We aim for a purity of propylene containing < 40 ppm (propyne+propadiene). It is clear that this requirement is dictated by the breakthrough of propadiene; see **Figure S23.**

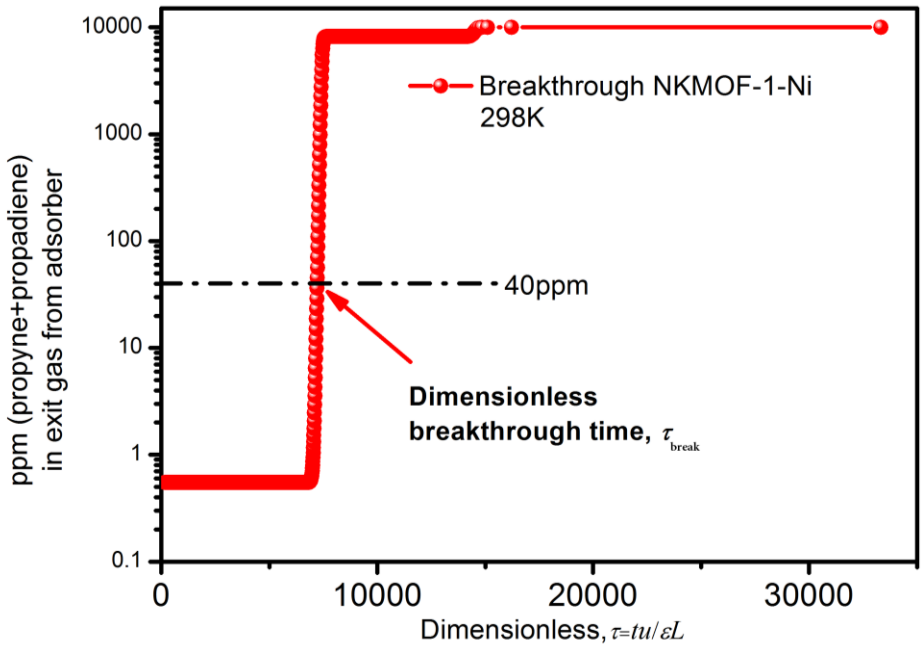

Figure S23. Simulation breakthrough curves of **NKMOF-1-Ni**

The dimensionless breakthrough time at which the ppm (propyne+propadiene) in product gas equals 40 ppm corresponds is τ_{break}. During the time interval 0 to τ_{break}, we can recover propylene from the outlet containing < 40 ppm (propyne + propadiene). From a material balance on the adsorber, we can determine the productivity of propylene with the desired purity < 40 ppm (propyne + propadiene).

The volumetric productivity, expressed mol/L of adsorbent in the packed bed, for the various MOFs are plotted in the Figure 3b as a function of τ_{break}. The highest productivity is achieved with **NKMOF-1-Ni**.

Breakthrough Experiment. The breakthrough experiments for propyne/propadiene/propylene (0.5/0.5/99) mixtures were carried out at a flow rate of 2 mL/min (298 K, 1 bar). Activated MOFs (about 1 g for each test) powder were packed into ϕ2×70 mm stainless steel column under pure N_2 atmosphere. The samples in the

column were compressed under the same condition and the column voidages are similar for different samples in order to compare the separation performance. The experimental set-up consisted of two fixed-bed stainless steel reactors. One reactor was loaded with the adsorbent, while the other reactor was used as a blank control group to stabilize the gas flow. The horizontal reactors were placed in a temperature controlled environment, maintained at 298 K. The flow rates of all gases mixtures were regulated by mass flow controllers, and the effluent gas stream from the column is monitored by a gas chromatography (TCD-Thermal Conductivity Detector, detection limit 0.1 ppm). Prior to the breakthrough experiment, we activated the sample by flushing the adsorption bed with helium gas for 30 min at proper temperature. Before each separation test, the adsorption bed was regenerated by He flow (50 mL/min) for 12 h at 363 K to ensure the totally removal of adsorbed gas.

The propylene productivity (q) is defined by the breakthrough amount of propylene, which is calculated by integration of the breakthrough curves $f(t)$ during a period from t_1 to t_2 where the propylene purity is higher than or equal to a threshold value p:

$$q = \frac{\mathrm{C}_i(C_3\mathrm{H}_6)}{\mathrm{C}_i(C_3\mathrm{H}_6) + \mathrm{C}_i(C_3\mathrm{H}_4)} \times \left(\int_{t1}^{t2} f(t)dt\right)$$

Table S19 Crystal data of **propyne@NKMOF-1-Cu** (Crystals of **NKMOF-1-Cu** were exposed to pure propyne gas).

propyne@NKMOF-1-Cu.	
Identification code	propyne@NKMOF-1-Cu

Empirical formula	$C_{11}H_8Cu_2N_4S_4$
Formula weight	451.53
Temperature/K	120(2)
Crystal system	triclinic
Space group	P-1
a/Å	6.82639(12)
b/Å	6.82639(12)
c/Å	16.5083(5)
α/°	90
β/°	90
γ/°	90
Volume/Å^3	769.28(3)
Z	2
ρ_{calc}g/cm^3	1.949
μ/mm^{-1}	3.301
F(000)	448.0
Radiation	MoK$_\alpha$ (λ = 0.71073)
2Θ range for data collection/°	5.968 to 52.974
Index ranges	$-8 \le h \le 8$, $-8 \le k \le 8$, $-20 \le l \le 20$
Reflections collected	11145
Independent reflections	3181 [R_{int}= 0.0456, R_{sigma}= 0.0454]
Data/restraints/parameters	3181/126/222
Goodness-of-fit on F^2	1.022
Final R indexes [I>=2σ (I)]	R_1= 0.0271, wR_2= 0.0599
Final R indexes [all data]	R_1= 0.0379, wR_2= 0.0649
Largest diff. peak/hole / e Å^{-3}	0.58/-0.36

Table S20 Crystal data of **propadiene@NKMOF-1-Cu** (Crystals of **NKMOF-1-Cu** were exposed to pure propadiene gas).

	propadiene@NKMOF-1-Cu
Identification code	propadiene@NKMOF-1-Cu
Empirical formula	$C_{11}H_8Cu_2N_4S_4$
Formula weight	451.53
Temperature/K	120(2)
Crystal system	triclinic
Space group	P-1
a/Å	6.8324(3)
b/Å	6.8324(3)
c/Å	16.4045(17)
α/°	90
β/°	90
γ/°	90
Volume/Å3	765.79(9)
Z	2
ρcalcg/cm3	1.958
μ/mm-1	3.316
F(000)	448.0
Radiation	MoK_α ($\lambda = 0.71073$)
2Θ range for data collection/°	5.962 to 57.818
Index ranges	$-9 \leq h \leq 9$, $-9 \leq k \leq 6$, $-22 \leq l \leq 22$
Reflections collected	6032
Independent reflections	3455 [Rint= 0.0643, Rsigma= 0.1403]
Data/restraints/parameters	3455/34/205
Goodness-of-fit on F2	1.020
Final R indexes [I>=2σ (I)]	R1= 0.0649, wR2= 0.1176
Final R indexes [all data]	R1= 0.1401, wR2= 0.1440
Largest diff. peak/hole / e Å-3	1.12/-0.88

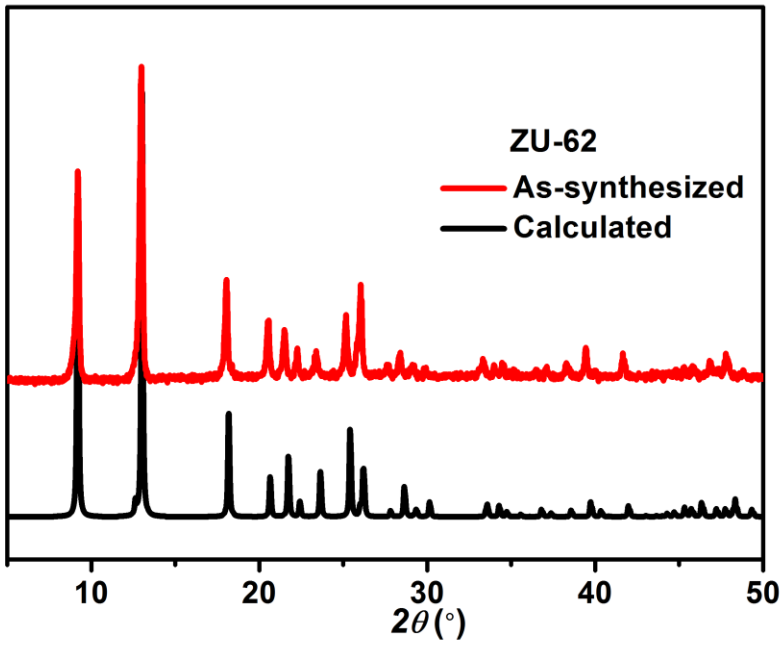

Figure S24. PXRD patterns of calculated and as-synthesized **ZU-62**.

Notation

p_i	partial pressure of species i in mixture, Pa
q_i	component molar loading of species i, mol kg^{-1}
q_A	gravimetric uptake of species A, mol kg^{-1}
q_{sat}	saturation loading, mol kg^{-1}
Q_A	volumetric uptake of species A, mol m^{-3}
ΔQ	separation potential, mol L^{-1}
L	length of packed bed adsorber, m
t	time, s
T	absolute temperature, K
u	superficial gas velocity in packed bed, m s^{-1}
y_A	gas phase mole fraction of species A, dimensionless
y_B	gas phase mole fraction of species B, dimensionless

Greek letters

ε voidage of packed bed, dimensionless

τ time, dimensionless

ρ framework density, kg m^{-3}

Subscripts

A referring to component A

B referring to component B

t referring to total mixture

References

1. Y.-L. Peng, T. Pham, P. Li, T. Wang, Y. Chen, K.-J. Chen, K. A. Forrest, B. Space, P. Cheng, M. J. Zaworotko, Z. Zhang, *Angew. Chem., Int. Ed*. **2018**, *57*, 10971-10975.
2. L. Yang, X. Cui, Q. Yang, S. Qian, H. Wu, Z. Bao, Z. Zhang, Q. Ren, W. Zhou, B. Chen, H. Xing, *Adv. Mater*. **2018**, *30*, 1705374.
3. L. Yang, X. Cui, Z. Zhang, Q. Yang, Z. Bao, Q. Ren, H. Xing, *Angew. Chem., Int. Ed*. **2018**, *130*, 13329-13333.
4. R. T. Yang, **1986**, Imperial College Press: London.
5. H. Pan, J. A. Ritter, P. B. Balbuena, *Langmuir* **1998**, *14*, 6323-6327.
6. E. T. Whittaker, G. Robinson, The Calculus of Observations: A Treatise on Numerical Mathematics, 4th Ed.; Dover: New York, **1967**, pp. 84-87.

7. T. Pham, K. A. Forrest, D. M. Franz, Z. Guo, B. Chen, B. Space, *Phys. Chem. Chem. Phys*. **2017**, *19*, 18587-18602.

8. G. Kresse, J. Hafner, *Phys. Rev. B*. **1993**, *7*, 558-561.

9. G. Kresse, J. Furthmüller, *Phys. Rev. B.* **1996**, *54*, 11169-11186.

10. P. E. Blöchl, *Phys. Rev. B.* **1994**, *50*, 17953-17979.

11. G. Kresse, D. Joubert, *Phys. Rev. B*. **1999**, *59*, 1758-1775.

12. J. P. Perdew, K. Burke, M. Ernzerhof, *Phys. Rev. Lett.* **1997**, *78*, 1396.

13. S. Grimme, *J. Comput. Chem*. **2006**, *27*, 1787-1799.

14. N. Metropolis, A. W. Rosenbluth, M. N. Rosenbluth, A. H. Teller, *J. Chem. Phys*. **1953** *21*, 1087-1092.

15. P. P. Ewald, *Ann. Phys.* **1921**, *369*, 253-287.

16. B. A. Wells A. L. Chaffee, Wells, *J. Chem. Theory Comput*. **2015**, *11*, 3684-3695 .

17. J. Applequist, J. R. Carl, K.-K. Fung, *J. Am. Chem. Soc.* **1972**, *94*, 2952-2960.

18. B. Thole, *Chem. Phys*. **1981**, *59*, 341-350.

19. K. A. Bode, J. Applequist, *J. Phys. Chem*. **1996**, *100*, 17820-17824.

20. K. McLaughlin, C. R. Cioce, T.Pham, J. L. Belof, B. Space, *J. Chem. Phys*. **2013**, *139*, 184112.

21. J. L. Belof, B. Space, Massively Parallel Monte Carlo (MPMC). Available on GitHub. https://github.com/mpmccode/mpmc, **2012**.

22. L. E. Chirlian, M. M. Francl, *J. Comput. Chem*. **1987**, *8*, 894-905.

23. C. M. Breneman, K. B. Wiberg, *J. Comput. Chem*. **1990**, *11*, 361-373.

24. P. T. Van Duijnen, M. Swart, *J. Phys. Chem*. A. **1998**, *102*, 2399-2407.

25. A. J. Misquitta, A. J. Stone, *J. Chem. Theory Comput*. **2008**, *4*, 7–18.

26. F. Neese, *WIREs Comput. Mol. Sci*. **2012**, *2*, 73-78.

27. R. Krishna, *RSC Adv.* **2017**. *7*, 35724-35737.

28. R. Krishna, *Microporous Mesoporous Mater.* **2014**, *185*, 30-50.

29. R. Krishna, *RSC Adv.* **2015**, *5*, 52269-52295.

30. R. Krishna, *Sep. Purif. Technol.* **2018**, *194*, 281-300.